

Synthetic Methods | Hot Paper |

Alkaline-Earth-Catalysed Cross-Dehydrocoupling of Amines and Hydrosilanes: Reactivity Trends, Scope and Mechanism

Clément Bellini,^[a] Vincent Dorcet,^[b] Jean-François Carpentier,^{*,[a]} Sven Tobisch,^{*,[c]} and Yann Sarazin^{*,[a]}

Abstract: Alkaline-earth (Ae = Ca, Sr, Ba) complexes are shown to catalyse the chemoselective cross-dehydrocoupling (CDC) of amines and hydrosilanes. Key trends were delineated in the benchmark couplings of Ph₃SiH with pyrrolidine or tBuNH₂. Ae{E(SiMe₃)₂}₂·(THF)_x (E = N, CH; x = 2–3) are more efficient than {N[^]N}Ae{E(SiMe₃)₂}·(THF)_n (E = N, CH; n = 1–2) complexes (where {N[^]N}⁻ = {ArN(σ-C₆H₄)C(H)=NAr}⁻ with Ar = 2,6-*i*Pr₂-C₆H₃) bearing an iminoanilide ligand, and alkyl precatalysts are better than amido analogues. Turnover frequencies (TOFs) increase in the order Ca < Sr < Ba. Ba{CH(SiMe₃)₂}₂·(THF)₃ displays the best performance (TOF up to 3600 h⁻¹). The substrate scope (>30 products) includes diamines and di(hydrosilane)s. Kinetic analysis of the Ba-promoted CDC of pyrrolidine and Ph₃SiH shows that 1) the ki-

netic law is rate = k[Ba]¹[amine]⁰[hydrosilane]¹, 2) electron-withdrawing *p*-substituents on the arylhydrosilane improve the reaction rate and 3) a maximal kinetic isotopic effect (*k*_{SiH}/*k*_{SiD} = 4.7) is seen for Ph₃SiX (X = H, D). DFT calculations identified the prevailing mechanism; instead of an inaccessible σ-bond-breaking metathesis pathway, the CDC appears to follow a stepwise reaction path with N–Si bond-forming nucleophilic attack of the catalytically competent Ba pyrrolide onto the incoming silane, followed by rate limiting hydrogen-atom transfer to barium. The participation of a Ba silyl species is prevented energetically. The reactivity trend Ca < Sr < Ba results from greater accessibility of the metal centre and decreasing Ae–N_{amide} bond strength upon descending Group 2.

Introduction

The catalysis of cross-dehydrocoupling (CDC) reactions between E–H and E'–H moieties leading to the formation of E–E' bonds and release of dihydrogen as a by-product (E and E' are electronegative (N, O, P) and more electropositive (B, Si) *p*-block elements, respectively) is attracting growing interest in main-group chemistry.^[1] The resulting molecular or macromolecular species are useful as emissive materials, high-per-

formance elastomers, synthetic precursors for ceramic thin films and monoliths, and in biomedicine.^[2]

The formation of N–Si bonds to yield silazanes is of interest to our research program. Silazanes are valuable as ligands in coordination chemistry,^[3] bases,^[4] silylating agents^[5] or protecting groups for amines, indoles and anilines in organic synthesis.^[6] In addition, some oligo- and polysilazanes make for excellent precursors of Si₃N₄ ceramics.^[7] Traditional processes for the production of silazanes require metalation of amines with alkali bases or aminolysis of chlorosilanes,^[7a,8] but these procedures involve the undesirable formation of stoichiometric amounts of salts or HCl by-products. The impetus is now shifting towards cost- and atom-efficient methods, such as the expedient catalytic N–H/H–Si CDC of hydrosilanes with HNR¹R² amines (R¹, R² = H, alkyl, aryl). Middle- and late-transition-metal compounds in which the low-valent metal centre can undergo oxidative addition, for example, Pd Al₂O₃-supported species and graphene-supported nanoparticles,^[9] [Ru₃(CO)₁₂] and [Rh₆(CO)₁₆] clusters,^[10] or discrete Ru²⁺,^[6b,d] Rh⁺^[6c,11] or Cr⁰^[12] complexes, first dominated the arena; a copper(I) system was also described.^[13] Notable results were later achieved with hard, oxophilic metal ions for which σ-bond metathesis or Si-to-metal hydride transfer are prominent mechanistic features. Some success was met in the 1990s with Cp₂TiMe₂,^[14] and more recently Al³⁺,^[15] Yb³⁺,^[16] Yb²⁺,^[17] U⁴⁺,^[18] Zn²⁺^[19] and especially Ae²⁺ (Ae = alkaline-earth metal)^[17c,20] catalysts have shown great promise. Additionally, B(C₆F₅)₃ is useful for the coupling of hydrosilanes with aromatic amines.^[6e]

[a] C. Bellini, Prof. Dr. J.-F. Carpentier, Dr. Y. Sarazin
Organometallics: Materials and Catalysis Department
Institut des Sciences Chimiques de Rennes
UMR 6226 CNRS—Université de Rennes 1
Campus de Beaulieu, 35042 Rennes (France)
E-mail: jean-francois.carpentier@univ-rennes1.fr
yann.sarazin@univ-rennes1.fr

[b] Dr. V. Dorcet
Centre de Diffractométrie des Rayons X
Institut des Sciences Chimiques de Rennes
UMR 6226 CNRS—Université de Rennes 1, 35042 Rennes (France)

[c] Dr. S. Tobisch
University of St Andrews, School of Chemistry, Purdie Building
North Haugh, St Andrews, KY16 9ST (UK)
E-mail: st40@st-andrews.ac.uk

Supporting information for this article is available on the WWW under <http://dx.doi.org/10.1002/chem.201504316>. It contains structural characterisation of the DFT-optimised key species involved in the various pathways examined, crystallographic data (including a CIF file) for complex **7-Ba**, NMR spectra and mass spectra of all new silazanes and NMR spectra for all new complexes.

Amongst these, alkaline-earth catalysts are particularly efficient, achieving high selectivity in the coupling of hydrosilanes and amines, hydrazines or ammonia. Harder's Ca-azametallacyclopropane $\text{Ca}(\text{HMPA})_3(\eta^2\text{-Ph}_2\text{CNPh})$ couples aliphatic amines or aniline to Ph_3SiH with a metal loading of 3–10 mol% at 20 °C in 0.5–24 h.^[17c] Sadow's $\{\text{To}^M\}\text{Mg}\{\text{N}(\text{SiMe}_3)_2\}$ ($\text{To}^M = \text{tris}(\text{oxazolonyl})\text{borato}$) couples primary amines, ammonia or hydrazine with phenyl-substituted hydrosilanes.^[20a] The kinetic rate law is first order in $[\text{silane}]$ and $[\text{precatalyst}]$ and zero order in $[\text{amine}]$; mechanistic investigations suggested that the reaction proceeds by a turnover-limiting nucleophilic attack of the Mg amide onto the silane followed by rapid hydride transfer from hypervalent Si to the Mg centre. Hill reported that the homoleptic amido precatalysts $\text{Ae}\{\text{N}(\text{SiMe}_3)_2\}_2$ ($\text{Ae} = \text{Mg, Ca, Sr}$) promote the CDC of hydrosilanes and aliphatic amines or bulky anilines at 20–60 °C (metal loading 5–10 mol%),^[20b] but no data was provided for their Ba congener. The Ca precatalyst performed substantially better than its Mg and Sr analogues, as exemplified in the coupling of Et_2NH with Ph_2SiH_2 . However, several subtleties associated with the bond polarity and charge density of the Ae ion became apparent upon mechanistic investigation. The kinetic rate law was first order in $[\text{metal}]$ and $[\text{amine}]$ and zero order in $[\text{silane}]$ for the Mg and Ca precatalysts, but it was second order in $[\text{metal}]$ and first order in $[\text{amine}]$ and $[\text{silane}]$ with the Sr one. In a recent communication, we reported that highly active and selective Ba complexes surpass their Ca and Sr analogues for chemoselective N–H/H–Si CDC reactions,^[20c] the main mechanistic features were delineated by a combination of experiments and DFT calculations. The full scope of this Ae-catalysed reaction is presented here, together with a thorough DFT analysis of the rival mechanistic pathways. A complete set of data that highlights the differences between Ca, Sr and Ba (ionic radius $r_{\text{ionic}} = 1.00, 1.18$ and 1.35 \AA , respectively) is provided.

Results and Discussion

Precatalyst synthesis

A broad range of Ae precatalysts, some devoid of bulky ancillary ligands and some stabilised instead by the bidentate iminoanilide $\{\text{N}^{\wedge}\text{N}\}^-$ ($\equiv [\text{ArN}(\text{o-C}_6\text{H}_4)\text{C}(\text{H})=\text{NAr}]^-$, $\text{Ar} = 2,6\text{-iPr}_2\text{-C}_6\text{H}_3$), were initially screened in the CDC of amines and hydrosilanes (1–8, Figure 1). Most were prepared according to known literature protocols. The silanido compounds $\text{Ae}(\text{SiPh}_3)_2(\text{THF})_3$ (**5-Sr**, **5-Ba**) and the heteroleptic complex $\{\text{N}^{\wedge}\text{N}\}\text{Ba}\{\text{N}(\text{SiMe}_2\text{H})_2\}(\text{THF})_2$ (**7-Ba**) were synthesised here for the first time. The pyrrolido complexes $\{\text{N}^{\wedge}\text{N}\}\text{Sr}\{\text{N}(\text{CH}_2)_4\}(\text{HN}(\text{CH}_2)_4)$ (**9-Sr**), in which some degree of stabilisation is ensured by a coordinated molecule of pyrrolidine ($\text{HN}(\text{CH}_2)_4$),^[21] and $\{\text{N}^{\wedge}\text{N}\}\text{Ba}\{\text{N}(\text{SiMe}_3)_2\}(\text{HN}(\text{CH}_2)_4)_2$ (**10-Ba**) were also prepared for the mechanistic studies.

The yellow complex **5-Sr** ($\delta_{295\text{Si}} = -12.14$ ppm) and the orange compound **5-Ba** ($\delta_{295\text{Si}} = -12.11$ ppm) were obtained in 32 and 86% yield (unoptimised), respectively, upon salt metathesis between AeI_2 and freshly prepared $\text{Ph}_3\text{SiK}^{[22]}$ (2 equiv) in THF.^[23] The orange complex **7-Ba** supported by the bulky bidentate iminoanilide $\{\text{N}^{\wedge}\text{N}\}^-$ was synthesised by a salt metathesis reaction of $\{\text{N}^{\wedge}\text{N}\}\text{H}$, anhydrous BaI_2 and $\text{KN}(\text{SiMe}_2\text{H})_2$ ^[24] (2 equiv) following a known one-pot protocol.^[25] The orange Sr pyrrolide complex **9-Sr** was prepared in pentane upon aminolysis of the alkyl complex **8-Sr** with excess pyrrolidine (3 equiv). On the other hand, treatment of **6-Ba** with pyrrolidine (2 equiv) merely afforded the bis-adduct **10-Ba** by displacement of THF, with no evidence for the release of $\text{HN}(\text{SiMe}_3)_2$ and formation of a Ba pyrrolide.^[26] Diagnostic resonances in its ^1H NMR spectrum include broad overlapping multiplets at $\delta = 2.49$ and 1.27 ppm (8H each, belonging to the coordinated pyrrolidine molecule and pyrrolide) and a broad singlet at $\delta = 0.94$ ppm for the two $\text{HN}_{\text{pyrrolidine}}$ acidic hydrogen atoms.^[21] The presence of $\text{N}(\text{SiMe}_2\text{H})_2^-$ moieties in **7-Ba** compared to the more traditional $\text{N}(\text{SiMe}_3)_2^-$ amido group in **6-Ba** is known to impart greater stability and kinetic inertness by formation of intramolecular $\text{Ba}\cdots\text{H}-\text{Si}$ β -agostic interactions, although this may at times come at the expense of catalytic efficacy.^[24,27] The agostic contact in **7-Ba** was detected spectroscopically: the

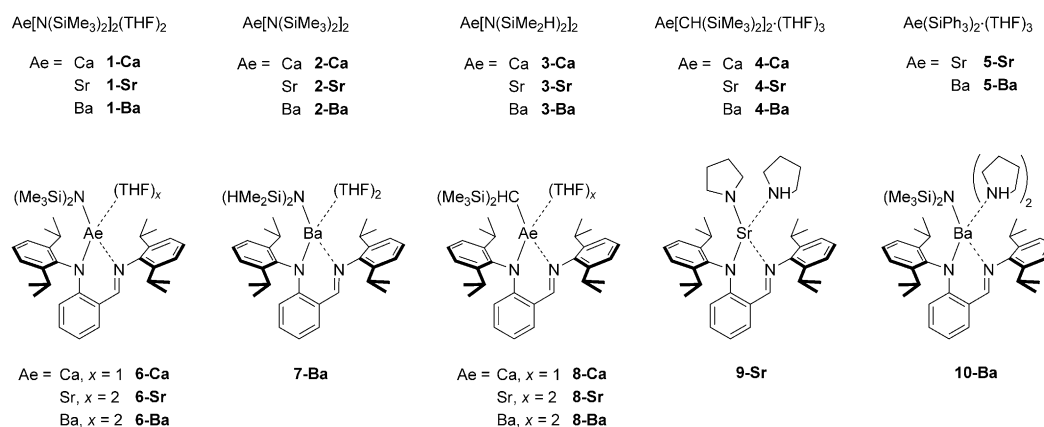


Figure 1. Ae precatalysts screened for N–H/H–Si CDC reactions.

coupling constant $^1J(\text{H},\text{Si})=160$ Hz in the ^1H NMR spectrum and the stretching frequency $\tilde{\nu}_{\text{Si-H}}=2004$ cm^{-1} in the FTIR spectrum of the complex both testified to the existence of agostic bonding of mild intensity. Agostic distortions are better visualised in the molecular solid-state structure of the complex determined by single-crystal X-ray diffraction (Figure 2). A large discrepancy is noted between the Ba2-N53-Si3 ($129.7(2)^\circ$) and Ba2-N53-Si4 ($105.31(19)^\circ$) angles. Moreover, the four atoms Ba2, N53, Si4 and H4 (with the Si4-H4 bond pointing towards the metal) are nearly perfectly coplanar, whereas Ba2, N53, Si3 and H3 are not. Both observations imply the presence of a single, mild Ba2...H4-Si4 agostic interaction,^[24–25,27–28] resulting in a formally six-coordinate Ba2 atom. By comparison, the two Ba-N-Si angles ($114.85(15)^\circ$ and $119.78(14)^\circ$) in **6-Ba** show less difference than the angles in **7-Ba**, and the Ba-N_{amide} bond length in **6-Ba** (2.623(3) Å) is elongated relative to that in **7-Ba** (2.601(4) Å).^[29]

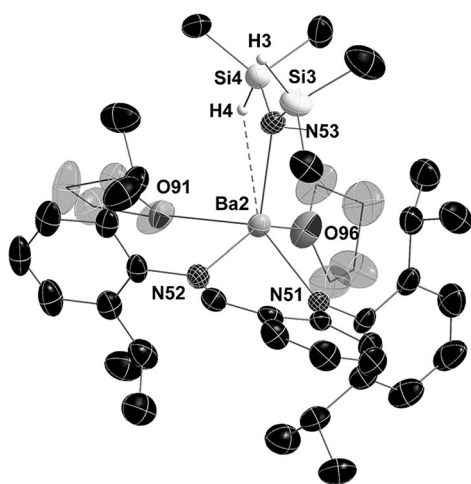
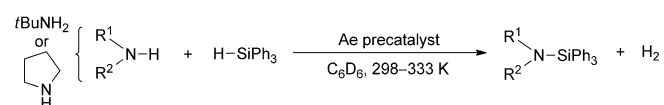


Figure 2. ORTEP representation (ellipsoids at the 50% probability level) of the molecular solid-state structure of $\{\text{N}^{\wedge}\text{N}\}\text{Ba}\{\text{N}(\text{SiMe}_2\text{H})_2\}\cdot(\text{THF})_2$ (**7-Ba**). Only one of the two independent but geometrically equivalent molecules found in the asymmetric unit, with the main component of the disordered THF molecule corresponding to O96, is depicted. Hydrogen atoms on the carbon atoms are omitted and the carbon atoms of the coordinated THF molecules are represented in a shaded tone for clarity. Selected bond lengths [Å] and angles [$^\circ$]: Ba2–N53 2.601(4), Ba2–N51 2.676(4), Ba2–N52 2.764(4), Ba2–O96 2.774(3), Ba2–O91 2.811(3); Si4–N53–Ba2 105.31(19), Si3–N53–Ba2 129.7(2).

Precatalyst screening

Complexes **1–9** were first assessed as precatalysts in N–H/H–Si CDC reactions in two benchmark reactions: the coupling of Ph_3SiH with the highly reactive pyrrolidine or with the more reluctant *tert*-butylamine (Scheme 1). From the results of this preliminary screening (Table 1), the following conclusions emerged:



Scheme 1. Benchmark CDC reactions for initial Ae precatalyst screening.

- 1) independently of the identity of the ligands, the catalytic activity increases systematically in the order $\text{Ca} < \text{Sr} < \text{Ba}$ (Table 1, entries 9, 10 and 11; entries 15, 16 and 18; entries 20, 21 and 22; entries 24, 25 and 26),^[30] the Ba precatalysts afforded unmatched overall turnover frequency (TOF) values calculated at 75–99% conversion up to 3600 h^{-1} (Table 1, entry 13).
- 2) the simple bis-amido complexes **1** are more effective than their direct heteroleptic counterparts **6** (Table 1, entry 9 versus 15, entry 10 versus 16, entry 11 versus 17); the same is true for the bis-alkyl complexes **4** and their heteroleptic derivatives **8** (Table 1, entry 14 versus 19, entry 22 versus 26).
- 3) the presence of coordinated THF molecules in bis-amido precatalysts bears no influence on the overall catalytic efficiency (Table 1, entry 3 versus 4, entry 10 versus 12).
- 4) the alkyl complexes are significantly more effective than their amido analogues (Table 1, entry 1 versus 2, entry 11 versus 13, entry 23 versus 26).
- 5) the complexes incorporating $\text{N}(\text{SiMe}_2\text{H})^-$ afford very little, if any, catalytic activity (Table 1, entries 5 and 7).
- 6) the bis-silanido complex **5-Sr** (Table 1, entry 6) is inactive, whereas the pyrrolido compound **9-Sr** is a competent catalyst (Table 1, entry 8),^[31] these observations have heavy implications regarding the nature of the reaction mechanism (see below).
- 7) even in the presence of excess Ph_3SiH (2 equiv versus the amine), the very mildly reactive *t*BuNH₂ solely affords the mono-coupled product *t*BuNHSiPh₃ with 100% chemoselectivity and no detectable formation of the decoupled product *t*BuN(SiPh₃)₂ (Table 1, entries 20–26), which highlights the difficulty in making RN(SiPh₃)₂ disilazanes (R = alkyl etc.) from primary amines by using this procedure.

From the foregoing, the bis-alkyl barium complex **4-Ba** is evidently the precatalyst of choice for this catalytic reaction. It is reasonably easy to prepare on a multi-gram scale compared with its more intricate heteroleptic derivative **8-Ba**. The more robust THF-coordinated amido analogue **1-Ba**, which is admittedly easier to synthesise, also exhibited impressive performance and therefore constitutes an excellent alternative. These two precatalysts were used to explore the substrate scope of the reaction.

It is disappointing, but not entirely unexpected, that complexes **3-Ba** and **7-Ba** bearing a tetramethyldisilazide moiety display very poor performance. Similar observations were made for the related Ca complex $\{\text{LO}\}\text{CaN}(\text{SiMe}_2\text{H})_2\cdot(\text{THF})$ complex ($\{\text{LO}\}^-$ = aminoether-phenolato ligand) used for the catalysis of intramolecular hydroamination reactions.^[27] It was demonstrated that this complex reacted with 2,2-dimethylpent-4-en-1-amine ($=\text{H}_2\text{NR}$) upon release of H_2 by self-catalysed dehydrocoupling to yield the catalytically inactive species $\{\text{LO}\}\text{CaN}(\text{SiMe}_2\text{H})(\text{SiMe}_2\text{NHR})_x$. One can assume that a similar deactivation process occurs in the present situation with **3-Ba** and **7-Ba**, especially because of the nature of the catalytic reaction under investigation here.

Table 1. Ae-catalysed CDC of amines and Ph₃SiH.^[a]

	R ¹ R ² N-H	Product	Precat.	N/Si/Ae	T [K]	t [min]	Conv. [%] ^[b]	TOF [h ⁻¹] ^[c]
1			1-Ca	20:20:1	298	2×60	29	3
2			4-Ca	20:20:1	298	2×60	74	7
3			1-Ba	20:20:1	298	2×60	91	9
4			2-Ba	20:20:1	298	2×60	87	9
5			3-Ba	20:20:1	298	2×60	3	<1
6			5-Sr	20:20:1	298	2×60	0	0
7			7-Ba	20:20:1	298	2×60	11	<1
8			9-Sr	20:20:1	298	2×60	92	9
9			1-Ca	400:400:1	298	15×60	72	19
10			1-Sr	400:400:1	298	15×60	99	26
11			1-Ba	400:400:1	298	15	99	1584
12			2-Sr	400:400:1	298	15×60	99	26
13			4-Ba	400:400:1	298	5	75	3600
14			4-Ba	400:400:1	298	15	99	1584
15			6-Ca	400:400:1	298	15×60	42	11
16			6-Sr	400:400:1	298	15×60	74	20
17			6-Ba	400:400:1	298	15	32	512
18			6-Ba	400:400:1	298	15×60	99	26
19			8-Ba	400:400:1	298	15	63	1008
20	<i>t</i> Bu-NH ₂		8-Ca	20:20:1	333	2×60	0	0
21			8-Sr	20:20:1	333	2×60	5	<1
22			8-Ba	20:20:1	333	2×60	25	3
23			1-Ba	20:20:1	333	2×60	50	5
24			4-Ca	20:20:1	333	2×60	9	1
25			4-Sr	20:20:1	333	2×60	82	8
26			4-Ba	20:20:1	333	2×60	95	10

[a] Reactions in C₆D₆ (0.5 mL), with [Ae]₀ = 10.0 mM and [amine] = 0.2 M for [amine]₀/[Ph₃SiH]₀/[precat.]₀ = 20:20:1 or 20:40:1, and [amine] = 4.0 M for [amine]₀/[Ph₃SiH]₀/[precat.]₀ = 400:400:1; reactions times are not optimised. In the case of *t*BuNH₂ (entries 20–26), the formation of *t*BuN(SiPh₃)₂ was never detected. [b] Conversion of the starting amine, as determined by ¹H NMR spectroscopy. [c] Overall TOF calculated at maximal conversion.

Reaction scope

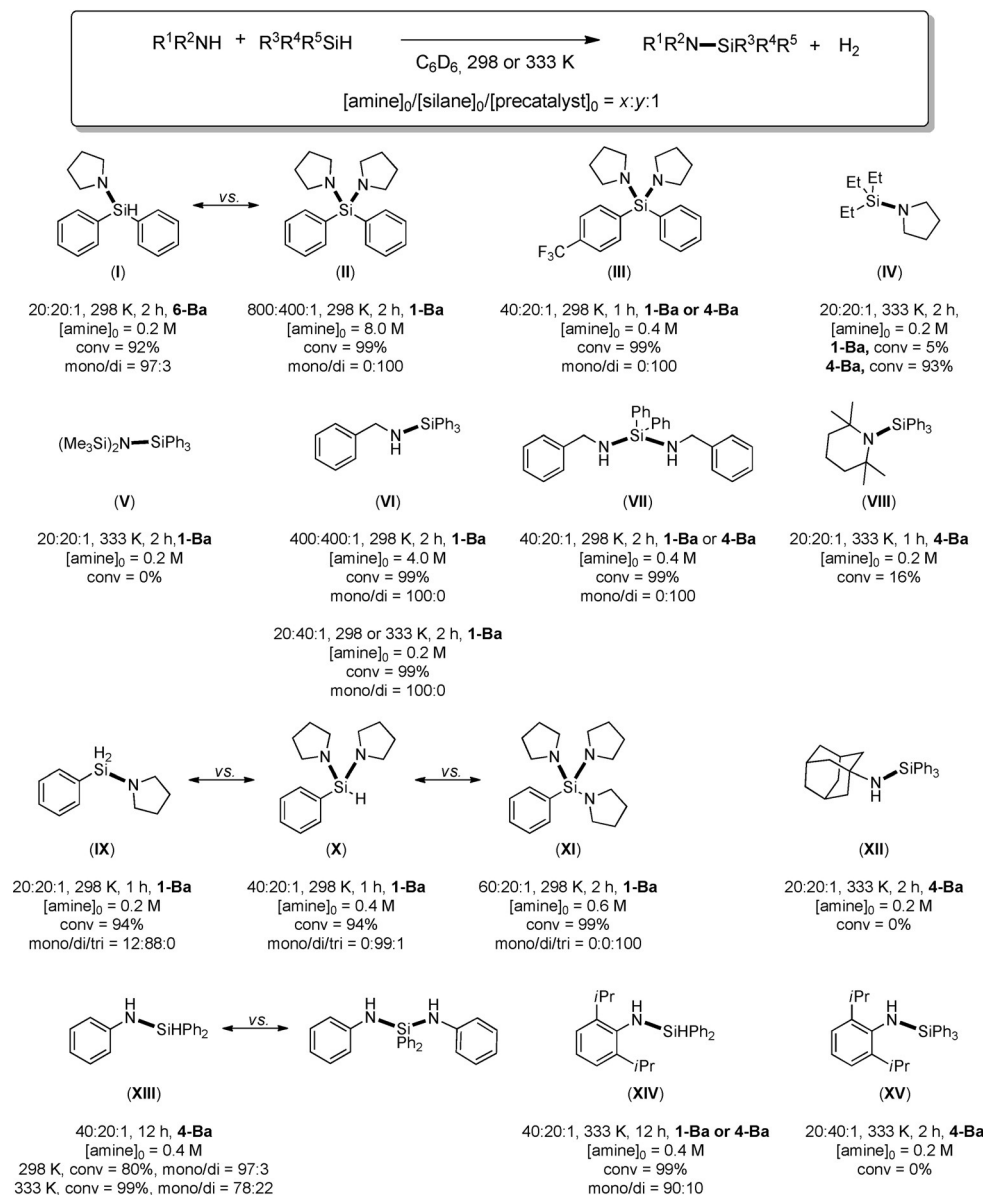
The substrate scope of the catalytic reaction was evaluated with precatalysts **1-Ba** and **4-Ba** (the heteroleptic and less-active precatalyst **6-Ba** was only used twice in specific cases for very reactive substrates) and a variety of silanes and amines. The results for this screening are summarised in Scheme 2 for reactions involving monoamines and mono(hydrosilane)s, and the coupling of di(hydrosilane)s with monoamines and that of diamines with mono(hydrosilane)s are collected in Schemes 3 and 4, respectively.^[32] The reactions were performed in C₆D₆ (identical outcomes were obtained for reactions carried out in C₆D₅Cl and in 5:1 mixtures of C₆D₆/1,2-C₆H₄F₂, which have higher dielectric constants than C₆D₆),^[33] and the substrate conversion was monitored by ¹H NMR spectroscopy. All new products were characterised by standard analytical methods (¹H, ¹³C and ²⁹Si NMR spectroscopy and mass spectrometry). Generally speaking, the chemoselectivity and measured conversions were excellent and, in the case of potentially difunctional substrates, the course of the reaction and specific formation of a given product could be controlled by judicious choice of the precatalyst (the more-active precatalyst **4-Ba** was used for more reluctant reactions and/or substrates)

and experimental conditions (i.e. temperature, reaction time and substrate loading).

Arylhydrosilanes (Ph₃SiH, Ph₂SiH₂ or PhSiH₃) react very quickly with pyrrolidine (Scheme 2). The dihydrosilane Ph₂SiH₂ selectively yields Ph₂SiH(N(CH₂)₄) (I) or Ph₂Si(N(CH₂)₄)₂ (II) depending on the reaction conditions; the corresponding TON (up to 800 equiv of amine per metal) are otherwise unmatched. With **1-Ba** as the precatalyst, reaction with PhSiH₃ leads to facile formation of PhSiH(N(CH₂)₄)₂ (X) or even to the tri-coupled PhSi(N(CH₂)₄)₃ (XI), but the high reactivity of the PhSiH₃/pyrrolidine pair of substrates precludes clean formation of the mono-coupled product PhSiH₂(N(CH₂)₄) (IX). The presence of a *para* electron-withdrawing group increases the reaction rate, as seen for (*p*-CF₃-C₆H₄)PhSi(N(CH₂)₄)₂ (III): complete conversion is achieved within 1 h (compare with the formation of I and II). This observation will be discussed in more detail in the kinetic and mechanistic analysis of this catalytic process (see below). Benzylamine is as good a substrate as pyrrolidine, with high chemoselectivity, TON and reaction rates being achieved at 298 K to afford (C₆H₅CH₂NH)SiPh₃ (VI) and (C₆H₅CH₂NH)₂SiPh₂ (VII). Such selectivity is remarkable, and formation of the *N*-di-coupled product (C₆H₅CH₂)N(SiPh₃)₂ was never observed. This suggests limited ability of (SiR₃)_xNH_{3-x} silazanes (*x* = 1, 2) to engage in CDC with hydrosilanes, a reckoning already made during the preliminary screening (see above) and further reinforced by the complete absence of V in the attempted catalysed coupling of Ph₃SiH and HN(SiMe₃)₂.

Aliphatic silanes are moderately reactive. The synthesis of Et₃Si(N(CH₂)₄) (IV) from triethylhydrosilane and pyrrolidine requires forcing conditions, even with **4-Ba** as the precatalyst. Bulky amines also react with great difficulty. With 2-adamantylamine (adam-NH₂), no conversion to (adam-NH)SiPh₃ (XII) was detected spectroscopically, and CDC of tetramethylpiperidine with Ph₃SiH only reached 16% conversion to VIII after 1 h at 333 K. Aromatic amines exhibit lower reactivity than aliphatic amines, presumably on account of their reduced nucleophilicity. Hence, 2,6-diisopropylaniline can be paired with Ph₂SiH₂ to give (2,6-*i*Pr₂-C₆H₃-NH)SiHPh₂ (XIV) with good selectivity after a prolonged reaction time at 333 K, but the corresponding coupling to generate XV from the bulkier Ph₃SiH failed entirely. The reactions with less-encumbered anilines proceeded more smoothly. Clean formation of (C₆H₅N)SiHPh₂ (XIII) was achieved at 298 K from a 40:20 mixture of aniline and Ph₂SiH₂, whereas a 78:22 mixture of XIII and its di-coupled derivative (C₆H₅N)₂SiPh₂ was obtained at 333 K; clean synthesis of this latter product could not be achieved under the chosen experimental conditions.

The reactivity of di(hydrosilane)s follows that detailed for mono(hydrosilane)s, and gives access to original di(silazane)s (Scheme 3). The reagent 1,2-bis(dimethylsilyl)ethane is rather unreactive. It undergoes CDC with pyrrolidine only after 12–15 h, and preferably at 333 K, to give mixtures of ((CH₂)₄N)Me₂-

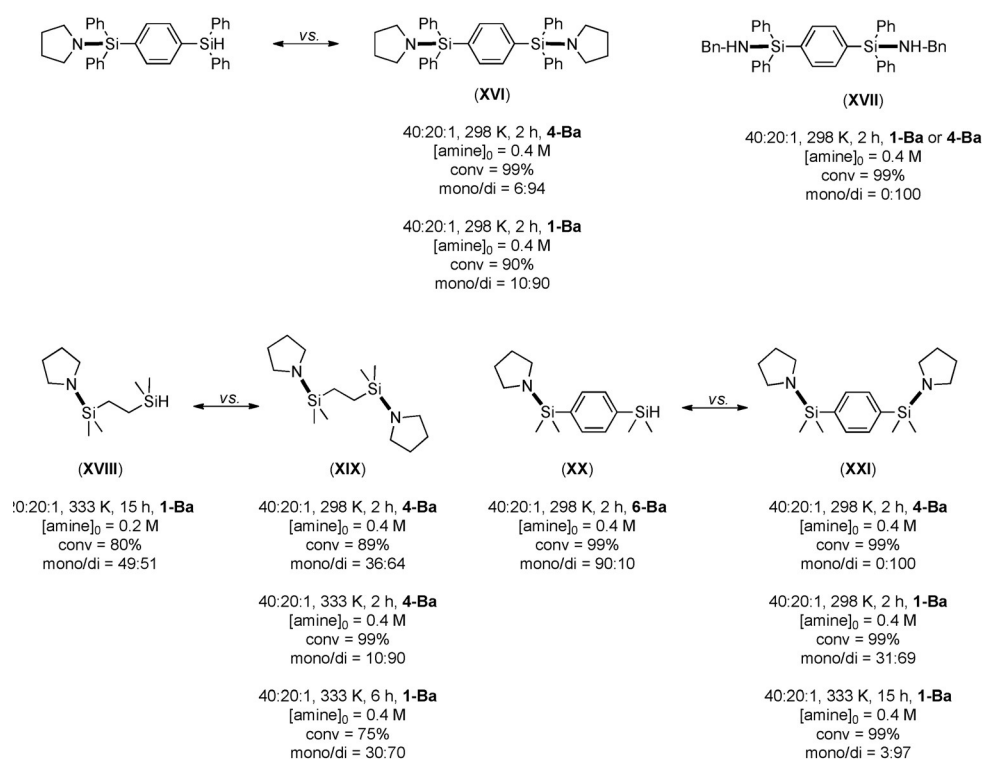
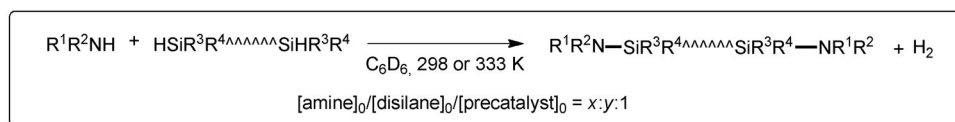


Scheme 2. Ba-catalysed CDC of mono(amines) and mono(hydrosilanes). Reactions were performed in C₆D₆ with precatalysts **1-Ba**, **4-Ba** or **6-Ba**. For each product (I–XV) the [amine]₀/[silane]₀/[precat.]₀ ratio, reaction temperature and time, precatalyst, substrate conversion (related to the conversion of the initial hydrosilane) and chemoselectivity between the mono-, di- and tri-coupled silazane products are indicated. Newly formed bonds are shown in bold.

SiCH₂CH₂SiHMe₂ (**XVIII**) and preponderantly its di-coupled analogue ((CH₂)₄N)Me₂SiCH₂CH₂SiMe₂(N(CH₂)₄) (**XIX**) with limited selectivity, even with precatalyst **4-Ba**. Greater reactivity is seen for 1,4-bis(diphenylsilyl)benzene, which couples twice with pyrrolidine or benzylamine under mild conditions to produce ((CH₂)₄N)Ph₂Si–C₆H₄–SiPh₂(N(CH₂)₄) (**XVI**) and (C₆H₅CH₂NH)SiPh₂–C₆H₄–SiPh₂(NHCH₂C₆H₅) (**XVII**), respectively, with good chemoselectivity. The reactivity of 1,4-bis(dimethylsilyl)benzene towards pyrrolidine is also rather satisfactory: **1-Ba** and **4-Ba** both afford clean access to ((CH₂)₄N)Me₂Si–C₆H₄–SiMe₂(N(CH₂)₄) (**XXI**), whereas **6-Ba** allows preponderant formation of the mono-coupled derivative, ((CH₂)₄N)SiMe₂–C₆H₄–SiMe₂H (**XX**).

The utilisation of diamines leads to the formation of valuable di(silazane)s (Scheme 4). Starting from 1,2-ethylenediamine, the

reaction can be oriented towards the formation of Ph₃SiNHCH₂CH₂NH₂ (**XXII**) or Ph₃SiNHCH₂CH₂NHSiPh₃ (**XXIII**) depending on the initial Ph₃SiH concentration; in no case was further coupling to (Ph₃Si)₂NCH₂CH₂NHSiPh₃ or even (Ph₃Si)₂NCH₂CH₂N(SiPh₃)₂ observed, another indication that –NHSiR₃ silazanes engage in CDC with hydrosilanes at best with great difficulty. From an *N,N'*-dimethylethylenediamine/Ph₃SiH feed ratio of 20:40, precatalysts **1-Ba** (at 298 K) and **4-Ba** (at 333 K) gave the mono-coupled Ph₃Si(Me)NCH₂CH₂NHMe (**XXV**) and the di-coupled Ph₃Si(Me)NCH₂CH₂N(Me)SiPh₃ (**XXVI**), respectively. Similarly, on adjusting the initial hydrosilane content of the reaction mixture, CDC of Ph₃SiH with piperazine at 298 K catalysed by **1-Ba** readily affords the mono- and di-coupled products, **XXVIII** and **XXIX**, with high chemoselectivity. By pairing *N,N'*-dibenzylethylenediamine with Ph₃SiH, Ph₃Si(Bn)-



Scheme 3. Ba-catalysed CDC of amines and di(hydrosilanes). Reactions were carried out in C₆D₆, using precatalysts **1-Ba**, **4-Ba** or **6-Ba**. For each product (**XVI**–**XXI**) the [amine]₀/[di(hydrosilane)]₀/[precatalyst]₀ ratio, reaction temperature and time, precatalyst, substrate conversion (related to the conversion of the initial di(hydrosilane)) and chemoselectivity between mono-, di- and tri-coupled silazane products are indicated. Newly-formed bonds are shown in bold.

NCH₂CH₂NHBn (**XXXI**) and Ph₃Si(Bn)NCH₂CH₂N(Bn)SiPh₃ (**XXXII**) can be accessed, although the selectivity towards **XXXI** was only moderate (83%). Diamines such as 1,4-phenylenedimethanamine and its *N,N'*-dimethyl-substituted congeners display mixed reactivity towards with Ph₃SiH. The di-coupled compounds Ph₃SiHNCH₂–C₆H₄–CH₂NHSiPh₃ (**XXIV**) and Ph₃Si(Me)NCH₂–C₆H₄–CH₂N(Me)SiPh₃ (**XXVII**) could be obtained smoothly with excellent selectivity. However, BnHNCH₂–C₆H₄–CH₂NHBn is far less reactive: the mono-coupled Bn(Ph₃Si)NCH₂–C₆H₄–CH₂NHBn (**XXX**) is formed exclusively but in poor yield (16%), even at 333 K with precatalyst **4-Ba**.^[34]

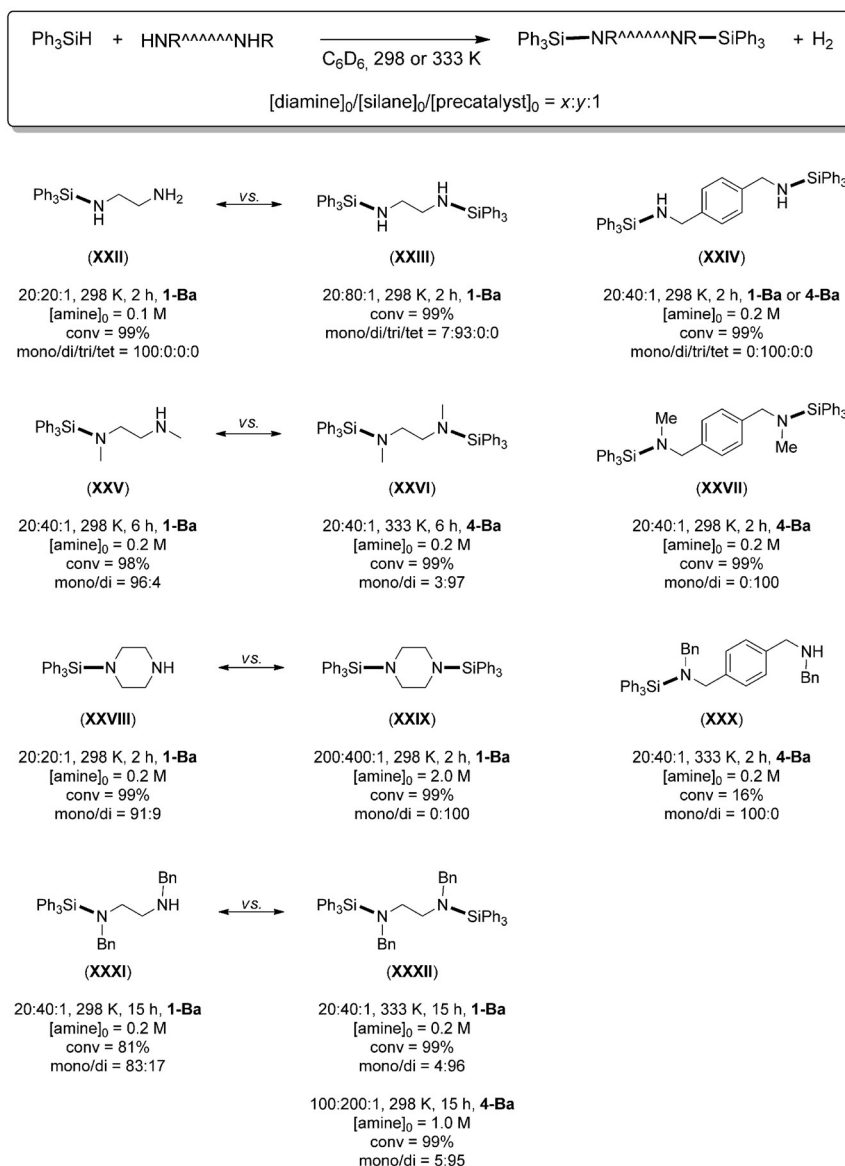
Overall, the Ba precatalysts **1-Ba** and **4-Ba** display a remarkable combination of productivity, activity and chemoselectivity in N–H/H–Si CDC reactions, and they give access to a wide range of original mono- and disilazanes. Notably, several of these products still possess N–H and/or Si–H reactive functional groups, which renders them useful synthetic intermediates that could be used for further functionalisation reactions. The performance displayed by **1-Ba** and **4-Ba** in the CDC of ditopic diamines and di(hydrosilanes) suggests that they might be good precatalysts for dehydrogenative polymerisation to afford polycarbosilazanes; for instance, we have prepared low

molecular weight polymers (*M_n* = 3–10 × 10³ g mol^{–1}) from *N,N'*-dibenzylethylenediamine and Ph₂SiH₂.^[32]

Kinetic analysis

Kinetic investigations were carried out to improve our understanding of these Ae-mediated N–H/H–Si CDC reactions. The main lines of the analysis of the coupling of pyrrolidine with Ph₃SiH, our benchmark substrates, catalysed by the bulky amido precatalyst **6-Ba** (**6-Ba** is less active than **1-Ba** and **4-Ba** and lends itself well to monitoring the substrate conversion by ¹H NMR spectroscopy) were reported in our earlier communication.^[20c] They are recalled here, together with comparative data for the Ca, Sr and Ba precatalysts.

From reactions carried out in C₆D₆ at 298 K, aimed at investigating the influence of the substrate concentrations ([pyrrolidine]₀ or [Ph₃SiH]₀) was varied over a 21-fold concentration range; Figures 3 and 4) and precatalyst concentration ([**6-Ba**]₀) was studied over a 15-fold concentration range; Figure 5), the second-order rate law corresponding to Equation (1) was established, with *k* = 4.802(13) × 10^{–3} M^{–1} s^{–1}.



Scheme 4. Ba-catalysed CDC of diamines and Ph₃SiH. Reactions were carried out in C₆D₆ with precatalysts **1-Ba** or **4-Ba**. For each product (**XXII-XXXII**) the [diamine]₀/[Ph₃SiH]₀/[precatalyst]₀ ratio, reaction temperature and time, precatalyst, substrate conversion (related to the conversion of the initial diamine) and chemoselectivity between the mono-, di- and tri-coupled silazane products are indicated. Newly-formed bonds are shown in bold.

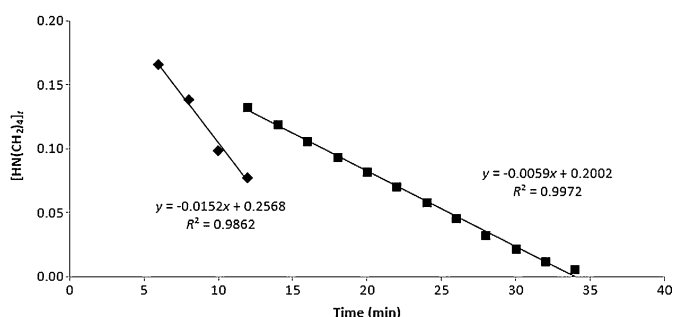


Figure 3. Plot of $[\text{HN}(\text{CH}_2)_4]_r = k_{\text{obs}} t$ as a function of time for the CDC of pyrrolidine and Ph₃SiH catalysed by **6-Ba**, showing partial zero-order kinetics in [pyrrolidine]. Conditions: HN(CH₂)₄ (8.0 μL, 0.1 mmol), Ph₃SiH (300 mg, 1.15 mmol), [**6-Ba**]₀ = 0.0179 M (◆, $k_{\text{obs}} = 2.53 \times 10^{-4} \text{ s}^{-1}$) or 0.0097 M (■, $k_{\text{obs}} = 9.83 \times 10^{-5} \text{ s}^{-1}$), $T = 298 \text{ K}$, C₆D₆.

$$R = -d[\text{pyrrolidine}]/dt = k [\text{6-Ba}]^1 [\text{pyrrolidine}]^0 [\text{Ph}_3\text{SiH}]^1 \quad (1)$$

An identical kinetic rate law was reported by Sadow and co-workers for N–H/H–Si dehydrocoupling reactions catalysed by $\{\text{To}^{\text{M}}\}\text{Mg}\{\text{N}(\text{SiMe}_3)_2\}_2$.^[20a] On the other hand, Hill and co-workers found different rate laws for the bis-amido precatalysts Ae{N–(SiMe₃)₂}₂, which were found to be of the form $R = k[\text{Ae}]^1[\text{pyrrolidine}]^1[\text{triphenylsilane}]^0$ for Ae = Mg and Ca, and $R = k[\text{Ae}]^2[\text{pyrrolidine}]^1[\text{triphenylsilane}]^1$ for Ae = Sr.^[20b]

For experiments run under otherwise identical conditions, a strong kinetic isotopic effect (KIE) of $k_{\text{Ph}_3\text{SiH}}/k_{\text{Ph}_3\text{SiD}} = 4.7(1)$ was measured for the coupling of Ph₃SiX (X = H, duplicate experiments; D, triplicate experiments from two batches of deuterated hydrosilane; the mean values of $k_{\text{Ph}_3\text{SiH}}$ and $k_{\text{Ph}_3\text{SiD}}$ were used to obtain the KIE) with HN(CH₂)₄ (Figure 6), that is, within the

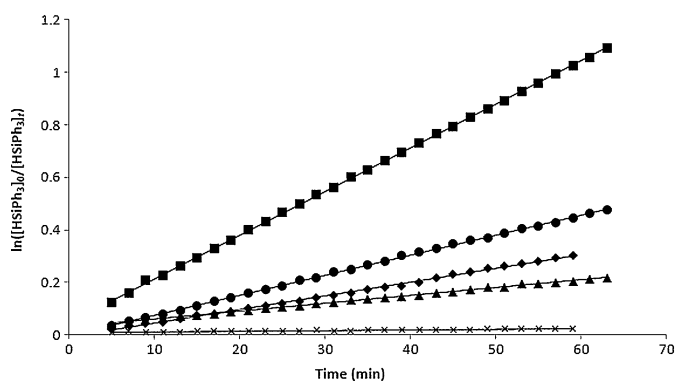


Figure 4. Plot of $\ln([\text{Ph}_3\text{SiH}]_0/[\text{Ph}_3\text{SiH}]_t) = k_{\text{obs}}t$ as a function of time for the CDC of pyrrolidine and Ph_3SiH catalysed by **6-Ba**, indicating partial first-order kinetics in $[\text{Ph}_3\text{SiH}]$. $T = 298\text{ K}$, C_6D_6 , $\text{HN}(\text{CH}_2)_4$ (160 μL , 2.0 mmol), Ph_3SiH (10.0 mg, 0.04 mmol), **[6-Ba]** = 4.0 mM (\times , $k_{\text{obs}} = 3.33 \times 10^{-6}\text{ s}^{-1}$), 11.0 mM (\blacktriangle , $k_{\text{obs}} = 4.67 \times 10^{-5}\text{ s}^{-1}$), 26.0 mM (\blacklozenge , $k_{\text{obs}} = 8.67 \times 10^{-5}\text{ s}^{-1}$), 30.0 mM (\bullet , $k_{\text{obs}} = 1.27 \times 10^{-4}\text{ s}^{-1}$) and 60.0 mM (\blacksquare , $k_{\text{obs}} = 2.77 \times 10^{-4}\text{ s}^{-1}$).

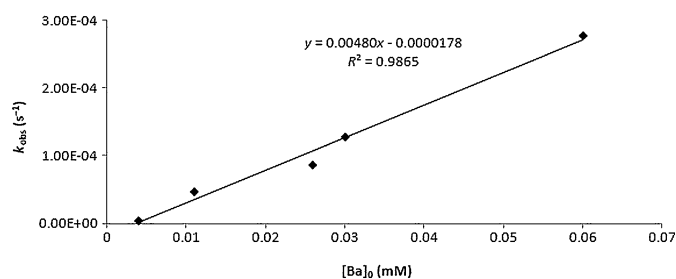


Figure 5. Linear plot of $k_{\text{obs}} = k[\mathbf{6-Ba}]$ as a function of $[\text{Ba}]_0$ for the CDC of pyrrolidine and Ph_3SiH catalysed by **6-Ba**, showing partial first-order kinetics in **[6-Ba]** with $k = 4.80 \times 10^{-3}\text{ M}^{-1}\text{ s}^{-1}$. Conditions: $\text{HN}(\text{CH}_2)_4$ (160 μL , 2.0 mmol), Ph_3SiH (10 mg, 0.04 mmol), **[6-Ba]** = 4.0, 11.0, 26.0, 30.0 and 60.0 mM, $T = 298\text{ K}$, C_6D_6 .

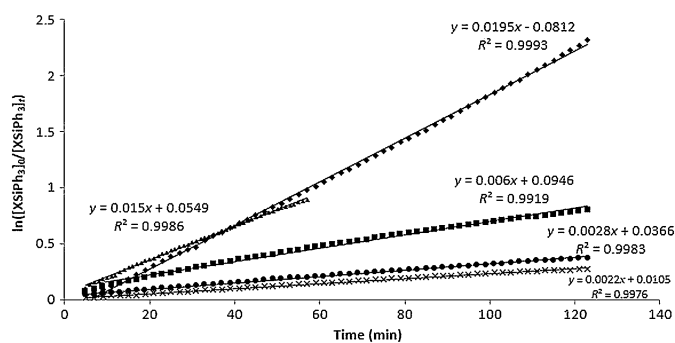


Figure 6. Plot of $\ln([\text{XSiPh}_3]_0/[\text{XSiPh}_3]_t) = k_{\text{obs}}t$ as a function of time for $X = \text{H}$ or D for the CDC of pyrrolidine and Ph_3SiX catalysed by **6-Ba**. Conditions: $\text{HN}(\text{CH}_2)_4$ (12.0 μL , 0.15 mmol), Ph_3SiH or Ph_3SiD (39 mg, 0.15 mmol) and **6-Ba** (4.4 mg, 5.0 μmol), $T = 298\text{ K}$, C_6D_6 . Ph_3SiH : $k_{\text{obs}} = 3.25 \times 10^{-4}$ (\bullet) and $2.50 \times 10^{-4}\text{ s}^{-1}$ (\blacktriangle); Ph_3SiD : $k_{\text{obs}} = 1.00 \times 10^{-4}$ (\blacklozenge) 4.67×10^{-5} (\bullet) and $3.67 \times 10^{-5}\text{ s}^{-1}$ (\times).

accuracy of the method the result is commensurate with the maximal theoretical value.^[35] No substantial KIE was detected for the amine, $k_{\text{HN}(\text{CH}_2)_4}/k_{\text{DN}(\text{CH}_2)_4} = 1.0(1)$. Both findings are consistent with the kinetic rate law and clearly imply that rupture of

the Si–H bond intervenes as a key event of the turnover-limiting step.

The activation parameters $\Delta H^\ddagger = 15.6(23)\text{ kcal mol}^{-1}$ and $\Delta S^\ddagger = -13.3(7.5)\text{ cal mol}^{-1}\text{ K}^{-1}$ ($\Delta G^\ddagger = 19.6(1)\text{ kcal mol}^{-1}$ at 298 K) were determined by an Eyring analysis, with six data points in the temperature range 293–318 K (Figure 7).^[36] The negative value of ΔS^\ddagger , diagnostic of an associative mechanism, is small relative to those given for other Mg–Sr CDC precatalysts,^[20a–b] this is possibly a consequence of the large radius of the Ba^{2+} ion ($r_{\text{ionic}} = 1.38\text{ \AA}$), which may induce a less-constrained arrangement in the transition state.

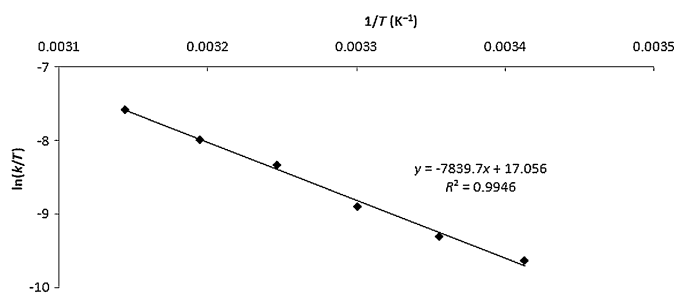


Figure 7. Eyring plot for the CDC of pyrrolidine and Ph_3SiH catalysed by **6-Ba**; k was determined from the plot of $\ln([\text{Ph}_3\text{SiH}]_0/[\text{Ph}_3\text{SiH}]_t) = k_{\text{obs}}t$ with $k_{\text{obs}} = k[\mathbf{6-Ba}]^1[\text{HN}(\text{CH}_2)_4]^0$. $\text{HN}(\text{CH}_2)_4$ (8.0 μL , 0.10 mmol), Ph_3SiH (26 mg, 0.10 mmol) and **6-Ba** (3.0 mg, 0.0034 mmol), C_6D_6 , $T = 293\text{--}318\text{ K}$.

A Hammett analysis was performed for the coupling of pyrrolidine with $\text{Ph}_2(p\text{-X-C}_6\text{H}_4)\text{SiH}$ ($X = \text{Me}$, OMe , F , and CF_3). It showed that in comparison with Ph_3SiH ($X = \text{H}$), the reaction rates increased very substantially with electron-withdrawing groups ($X = \text{F}$, CF_3) and decreased with electron-donating substituents ($X = \text{Me}$, OMe), in the order $X = \text{OMe} < \text{Me} < \text{H} < \text{F} < \text{CF}_3$ (Table 2). The Hammett plot [Eq. (2)] is a straight line with a positive slope of $\rho = 2.0(2)$ (Figure 8),^[37] which clearly indicates that the activation barrier of the catalytic event is lowered by electron-withdrawing p -substituents, presumably by stabilisation of a developing negative charge on the silicon atom.

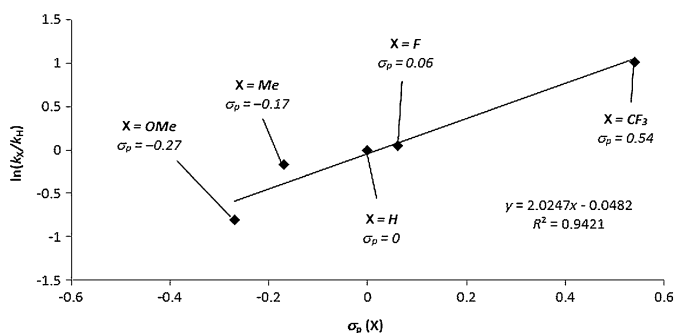


Figure 8. Hammett plot $\ln(k_x/k_H) = \sigma_p(X)\rho$ showing the reaction-rate acceleration with electron-withdrawing groups on the silane for the coupling of $\text{HN}(\text{CH}_2)_4$ and $\text{Ph}_2(p\text{-X-C}_6\text{H}_4)\text{SiH}$ ($X = \text{OMe}$, Me , H , F , or CF_3) catalysed by **6-Ba**. Experimental conditions: C_6D_6 (0.5 mL), $T = 298\text{ K}$, $\text{HN}(\text{CH}_2)_4$ (3.0 M), $\text{Ph}_2(p\text{-X-C}_6\text{H}_4)\text{SiH}$ (0.06 M).

Table 2. Hammett analysis for the CDC of pyrrolidine and $\text{Ph}_2(p\text{-X-C}_6\text{H}_4)\text{SiH}$ ($\text{X}=\text{H}$, Me, OMe, F and CF_3) catalysed by **6-Ba**.^[a]

X=OMe		X=Me		X=H		X=F		X=CF ₃	
[6-Ba] ₀ [mM]	k _{obs} [10 ⁵ s ⁻¹]	[6-Ba] ₀ [mM]	k _{obs} [10 ⁵ s ⁻¹]	[6-Ba] ₀ [mM]	k _{obs} [10 ⁵ s ⁻¹]	[6-Ba] ₀ [mM]	k _{obs} [10 ⁵ s ⁻¹]	[6-Ba] ₀ [mM]	k _{obs} [10 ⁵ s ⁻¹]
11.0	2.67	10.0	0.33	4.0	0.33	5.0	2.00	5.0	3.83
17.0	5.17	17.0	3.67	11.0	4.67	19.0	9.00	10.0	11.3
28.0	6.67	24.0	4.83	26.0	8.67	27.0	13.8	17.0	27.5
39.0	9.83	31.0	7.33	30.0	12.7	32.0	16.3	29.0	39.2
50.0	11.2	42.0	14.0	60.0	27.7	39.0	18.7	50.0	64.2

[a] Reactions in C₆D₆ (0.5 mL) at 298 K, [pyrrolidine]₀ = 3.0 M, [Ph₂(p-X-C₆H₄)SiH]₀ = 0.06 M.

$$\ln(k_X/k_H) = \sigma_p(X)\rho \quad (2)$$

This finding is consistent with the finding that the catalysed reaction leading to the formation of $(p\text{-CF}_3\text{-C}_6\text{H}_4)\text{PhSi}(\text{N}(\text{CH}_2)_4)_2$ (**III**) is more rapid than those yielding $\text{PhSiH}(\text{N}(\text{CH}_2)_4)_2$ (**I**) and $\text{Ph}_2\text{Si}(\text{N}(\text{CH}_2)_4)_2$ (**II**) (see Scheme 2).

From the qualitative experiments performed in the preliminary precatalyst screening (see Table 1) it had emerged that the catalytic activity increased in the order $\text{Ca} < \text{Sr} < \text{Ba}$. To better quantify this observation, the conversion of pyrrolidine during its CDC with Ph_3SiH catalysed by **6-Ca**, **6-Sr** or **6-Ba** at 298 K was monitored by NMR spectroscopy. The observed rate constants obtained from the semi-logarithmic plot of substrate conversion versus time (Figure 9) corroborated the earlier find-

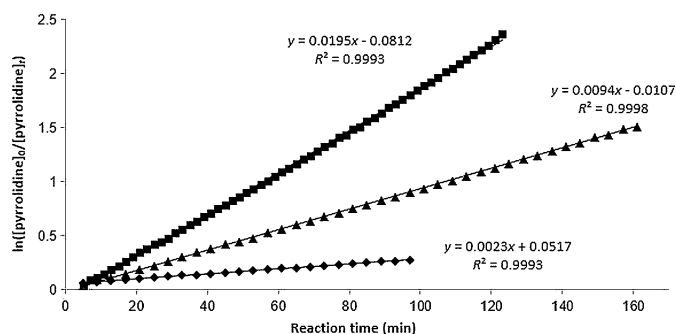


Figure 9. Comparative semi-logarithmic plot of pyrrolidine conversion versus reaction time for the CDC of pyrrolidine with Ph_3SiH catalysed by **6-Ca** (\blacklozenge , $k_{\text{obs}} = 3.83 \times 10^{-5} \text{ s}^{-1}$), **6-Sr** (\blacktriangle , $k_{\text{obs}} = 15.7 \times 10^{-5} \text{ s}^{-1}$) and **6-Ba** (\blacksquare , $k_{\text{obs}} = 32.5 \times 10^{-5} \text{ s}^{-1}$). Experimental conditions: $[\text{pyrrolidine}]_0 = 0.20 \text{ M}$, $[\text{pyrrolidine}]_0/[\text{Ph}_3\text{SiH}]_0/[\text{precatalyst}]_0 = 20:20:1$, C₆D₆ (0.5 mL), $T = 298 \text{ K}$.

ing that under the chosen experimental conditions, the rate constants increased by about one order of magnitude from calcium ($k_{\text{obs}} = 3.83 \times 10^{-5} \text{ s}^{-1}$) to strontium ($k_{\text{obs}} = 15.7 \times 10^{-5} \text{ s}^{-1}$) and to the most efficacious metal barium ($k_{\text{obs}} = 32.5 \times 10^{-5} \text{ s}^{-1}$).

For a given ligand set, the $\text{Ca} < \text{Sr} < \text{Ba}$ activity trend has often been reported for a variety of catalytic reactions; for instance in ring-opening polymerisation of cyclic esters,^[38] intermolecular hydroamination and hydrophosphination of activated alkenes^[29,39] and hydrophosphonylation of ketones.^[40] How-

ever, this must be mitigated because there is now a large body of evidence that shows activity varies in the order $\text{Ba} < \text{Sr} < \text{Ca}$ in the cyclohydroamination of aminoalkenes.^[41] Additionally, no clear trend emerges in some other cases, for example, in the hydroalkoxylation/cyclisation of alkynyl alcohols.^[42] The size of the Ae ion, its polarizability, electron surface potential and ability to bind incoming substrates and polarise their reactive bonds are all unquestionably some of the features that define the reactivity of the pertaining complexes and their catalytic ability.

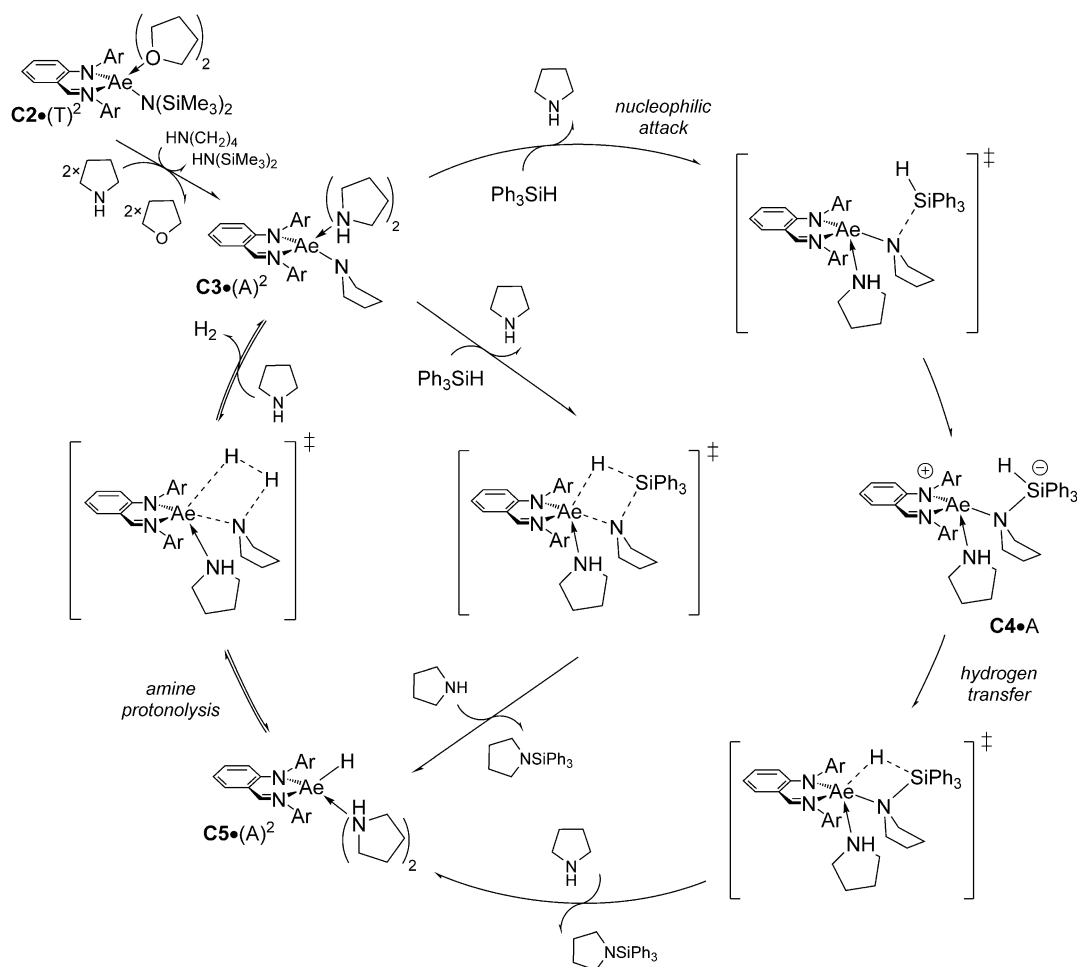
Computational investigations

To inform ourselves about which of the several conceivable mechanistic scenarios prevails, we embarked on a detailed computational analysis of alternative pathways for the CDC of pyrrolidine (**A**) and Ph_3SiH (**S**) catalysed by $\{\text{N}^{\wedge}\text{N}\}\text{Ba}\{\text{N}(\text{SiMe}_3)_2\} \cdot (\text{THF})_2$ (**6-Ba**, denoted thereafter as **C2**·(T)²). Various mechanistic pathways for a catalytically active Ba pyrrolide (Scheme 5) or alternatively a Ba silyl species (Scheme 6) have been thoroughly examined, the most accessible of which has been briefly characterised in our previous communication.^[20c] Taking the route for generation of the silazane product (**P**) that commences from the $\{\text{N}^{\wedge}\text{N}\}\text{Ae}$ pyrrolide by evolving through a $\{\text{N}^{\wedge}\text{N}\}\text{Ae}$ hydride intermediate that is converted back into the $\{\text{N}^{\wedge}\text{N}\}\text{Ae}$ pyrrolide compound thereafter (Scheme 5) as an example, the aforementioned kinetic data support both stepwise and concerted pathways, which further adds to the mechanistic diversity. The computational methodology employed (dispersion-corrected B97-D3 in conjunction with triple- ζ basis sets and a sound treatment of bulk solvent effects; see the Computational methodology in the Experimental section) adequately simulated authentic reaction conditions. The validity of the computational protocol to reliably map the free-energy landscape of Ae-mediated hydroelementation reactions has been substantiated before,^[39,41g] and this has allowed mechanistic conclusions with substantial predictive value to be drawn.

Herein we report the full account of examined pathways that are conceivable for delivery of the silazane product and also of the disilane by-product in the presence of precatalyst **6-Ba** (**C2**·(T)²). A second investigation scrutinizes the effect of the alkaline-earth metal ($\text{Ae} = \text{Ca}, \text{Sr}$) on the energetics of relevant elementary steps, which thereby provides invaluable insights into crucial structure–activity relationships of the CDC mediated by alkaline-earth iminoanilides.

Pathways starting from the $\{\text{N}^{\wedge}\text{N}\}\text{Ba}$ pyrrolide complex

A recent computational study^[39] of styrene hydroamination revealed that initial transformation of the $\{\text{N}^{\wedge}\text{N}\}\text{Ba}$ silylamide **C2**·(T)² precatalyst into the $\{\text{N}^{\wedge}\text{N}\}\text{Ba}$ pyrrolide compound **C3**, which is predominantly present as the bis-amine adduct **C3**·(A)² and exhibits no propensity towards dimer formation, is sufficiently facile kinetically. For catalytically competent silane adducts (**C3**·S·(A)ⁿ), a single adducted amine molecule greatly



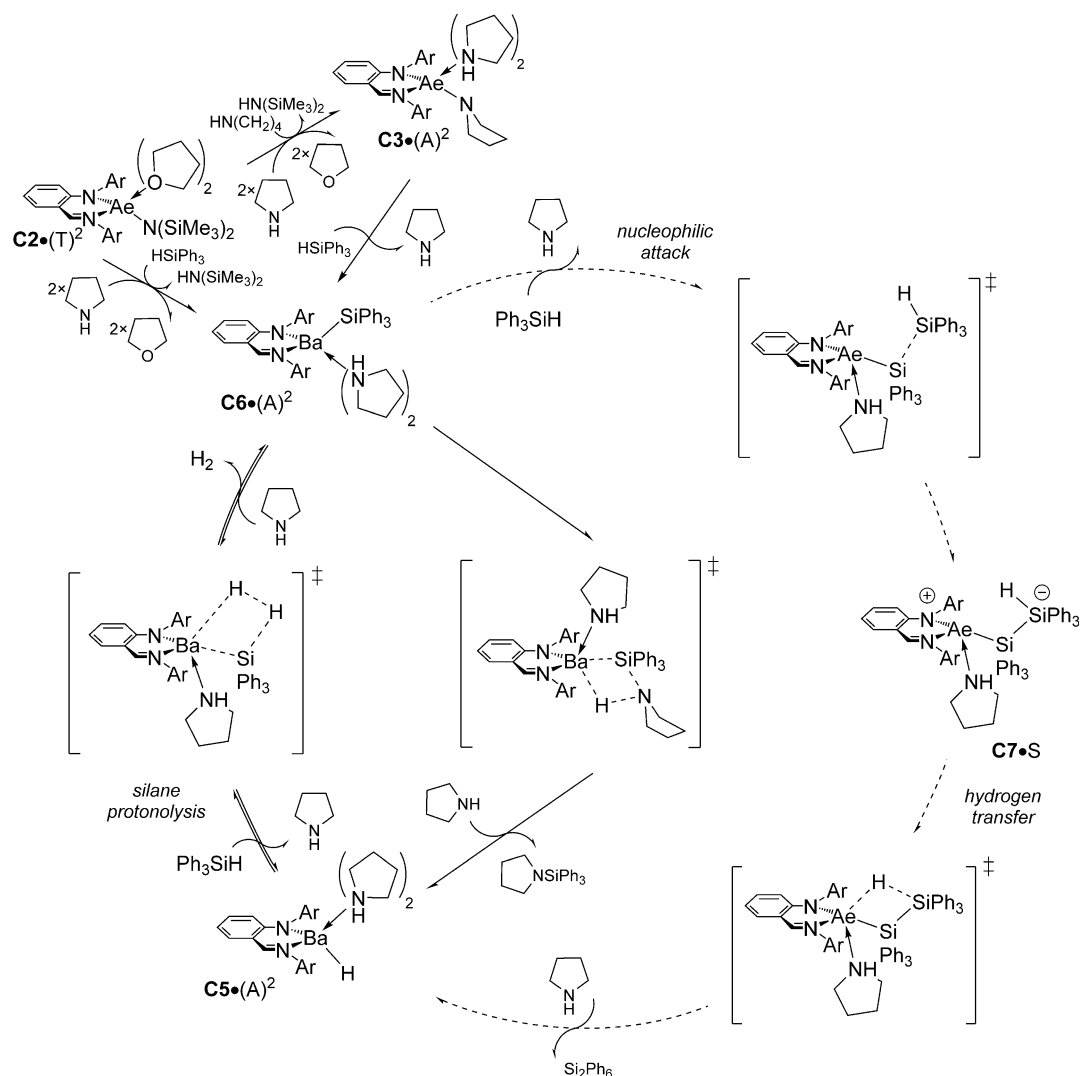
Scheme 5. Plausible mechanistic pathways for iminoanilide alkaline-earth-catalysed CDC of amines and silanes with $\{N^{\wedge}N\}Ae\{N(CH_2)_4\}$ (**C3**) as the catalytically competent compound and triphenylsilane (S) and pyrrolidine (A) substrates ($\{N^{\wedge}N\}^- = \{ArN(o-C_6H_4)C(H)=NAr\}^-$ with $Ar = 2,6\text{-}iPr_2\text{-}C_6H_3$).

stabilises **C3**-S, whereas the presence of the rather bulky Ph_3SiH compound makes it impossible for the $\{N^{\wedge}N\}Ba$ centre to accommodate another pyrrolidine molecule. Hence, **C3**-S and its mono-amine analogue **C3**-S•A are likely to participate in accessible pathways for catalyst turnover.

We start with the examination of a stepwise pathway (Scheme 5) for silazane formation that comprises nucleophilic attack of the $\{N^{\wedge}N\}Ae$ pyrrolide at the silane to furnish the transient silicate intermediate **C4** and subsequent hydrogen-atom transfer to the Ae centre, which gives rise to the $\{N^{\wedge}N\}Ae$ hydride **C5** with concomitant release of the silazane product P. The initial nucleophilic attack of a suitably nucleophilic pyrrolide nitrogen centre at S commencing from **C3**-S or **C3**-S•A, featuring only a loosely associated silane molecule, evolves through a transition-state (TS) structure that describes N–Si bond formation occurring outside of the immediate vicinity of the Ae centre at distances of 2.40–2.50 Å (see Figure S1 in the Supporting Information) for the emerging N–Si bond. Following the reaction path further, the TS structure decays into a metastable nucleophilic $\{N^{\wedge}N\}Ba$ silicate intermediate **C4** that features a five-coordinate silicon centre with an elongated Si–H linkage, thus indicating the distinct aptitude of **C4** to un-

dergo β -hydride elimination. No substantial structural reorganisation is required for transfer of the hydrogen atom from the five-coordinate silicon atom onto the Ae centre to proceed through a TS structure with distances of approximately 2.45 and 2.40 Å for vanishing Si–H and emerging Ba–H bonds (see Figure S1 in the Supporting Information), respectively, and generate the silazane product P and $\{N^{\wedge}N\}Ba$ hydride **C5**.

The most accessible pathway for stepwise silazane generation benefits from one associated pyrrolidine spectator molecule participating at all stages of the process (**C3**-S•A \rightarrow **C4**•A \rightarrow **C5**-P•A) on both kinetic and thermodynamic grounds (Figure 10). As far as the intrinsic reactivity is concerned, both the N–Si bond-forming nucleophilic attack of the Ba pyrrolide ($\Delta G^{\ddagger}_{int} = 4.5 \text{ kcal mol}^{-1}$ relative to **C3**-S•A) and the hydrogen-atom transfer ($\Delta G^{\ddagger}_{int} = 4.8 \text{ kcal mol}^{-1}$ relative to **C4**•A) are kinetically feasible to an astonishingly comparable amount. In terms of observable catalytic performance, the nucleophilic attack is predicted to be kinetically affordable ($\Delta G^{\ddagger} = 17.4 \text{ kcal mol}^{-1}$ relative to **C3**•(A)²), as is β -hydride elimination ($\Delta G^{\ddagger} = 19.0 \text{ kcal mol}^{-1}$ relative to **C3**•(A)²). The unfavourable thermodynamic profile of the nucleophilic attack favours **C3**-S•A over **C4**•A, which makes the second hydrogen-atom transfer more kineti-



Scheme 6. Plausible mechanistic pathways for iminoanilide alkaline-earth-catalysed CDC of amines and silanes, with $\{N^{\wedge}N\}Ae\{Si(C_6H_5)_3\}$ (**C6**) as the catalytically competent compound and triphenylsilane (**S**) and pyrrolidine (**A**) substrates. A rival pathway for silane homocoupling is also shown. ($\{N^{\wedge}N\}^- = \{ArN(o-C_6H_4)C(H)=NAr\}^-$ with $Ar = 2,6-iPr_2-C_6H_3$).

cally demanding. As can be anticipated, the incoming pyrrolidine moiety is likely to readily displace the silazane product **P** from $C_5 \cdot P \cdot A$.^[43] It renders the stepwise $C_3 \cdot (A)_2 \rightarrow C_3 \cdot S \cdot A \rightarrow C_4 \cdot A \rightarrow C_5 \cdot P \cdot A \rightarrow C_5 \cdot (A)_2$ silazane formation almost thermoneutral; the second hydrogen-atom transfer to Ba dictates the overall kinetics of this process.

On the other hand, despite all our efforts, a low-energy TS structure describing $Ba-N/Si-H$ σ -bond-breaking metathesis representing the concerted silazane-generating analogue (see Scheme 5) could not be located. Careful examination of the metathesis transformation with the aid of a reaction-path optimisation (chain-of-states) method starting from suitable estimated initial TS structures resulted in minimum-energy pathways that described either nucleophilic attack or hydrogen-atom transfer (depending on the initial TS starting point) as energetically prevalent alternatives. From this, one can conclude with some confidence that higher kinetic demands would be associated with the alternative concerted pathway,

thus this is unlikely to have any relevance for Ba catalyst turnover. Whether these findings hold true for more compact alkaline earths is analysed below.

The subsequent protonolysis of pyrrolidine by the $\{N^{\wedge}N\}Ba$ hydride converts **C5** back into the catalytically competent $\{N^{\wedge}N\}Ba$ pyrrolide for another catalyst turnover. The process starting from either the mono- or bis-pyrrolidine **C5** adduct evolves through a metathesis-type TS structure (see Figure S2 in the Supporting Information) that decays into amine-free and amine-adduct forms of the $\{N^{\wedge}N\}Ba$ pyrrolide compound through facile liberation of H_2 (1 equiv). The participation of one adducted amine spectator molecule facilitates the process greatly on thermodynamic and kinetic grounds, thereby paralleling the findings for the preceding nucleophilic attack step, and moreover causes the direct expulsion of H_2 after $TS[C_5 \cdot (A)_2 - C_3 \cdot A]$ is traversed. In light of a kinetically favourable ($\Delta G^\ddagger = 9.6 \text{ kcal mol}^{-1}$ relative to $C_5 \cdot (A)_2$) pyrrolidine protonolysis ($C_5 \cdot (A)_2 \rightarrow C_3 \cdot A + H_2(+A) \rightarrow C_3 \cdot (A)_2$) that is almost thermoneu-

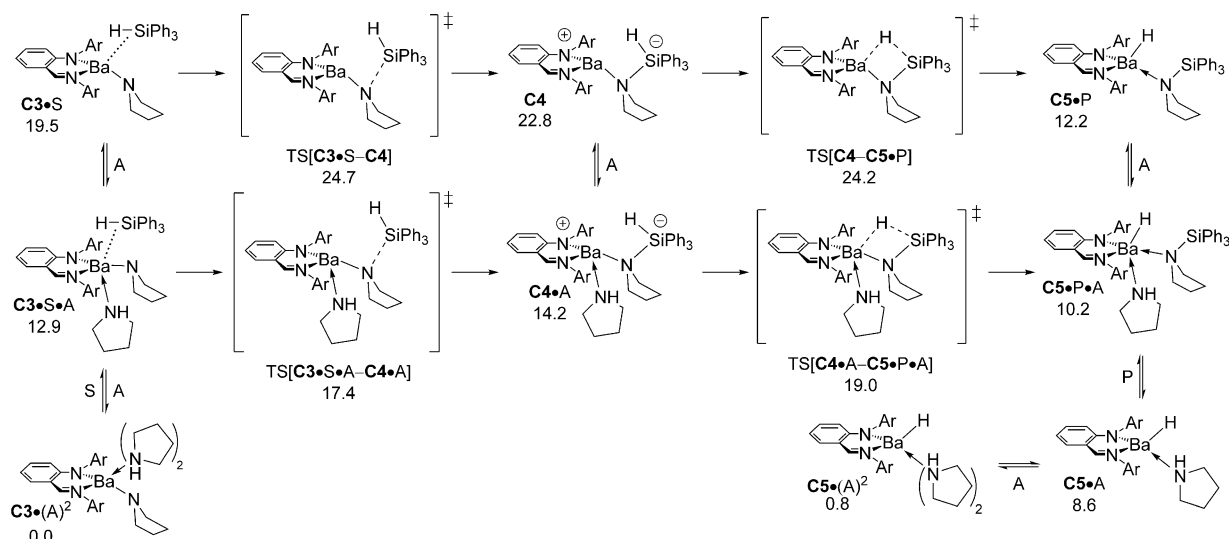


Figure 10. Nucleophilic attack of the $\{N^{\wedge}N\}Ba$ pyrrolide **C3** at Ph_3SiH (**S**) together with subsequent hydrogen-atom transfer to barium at the transient silicate intermediate **C4** to afford $\{N^{\wedge}N\}Ba$ hydride **C5** and the silazane product (**P**).^[43,44a] Energies are given in $kcal\ mol^{-1}$.

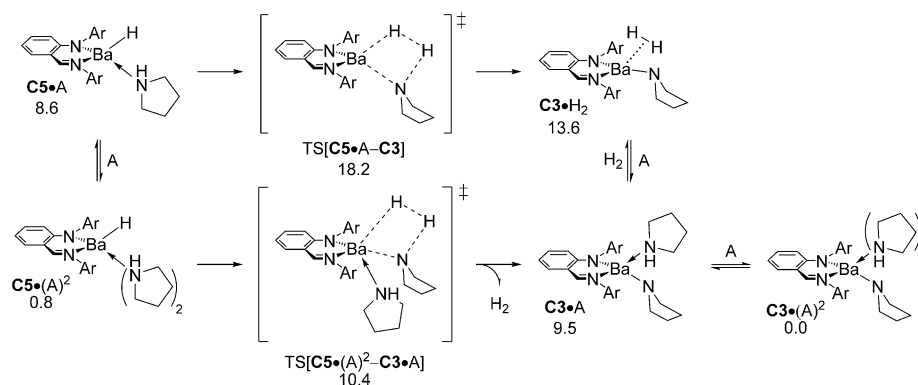


Figure 11. Protonolysis of pyrrolidine by $\{N^{\wedge}N\}Ba$ hydride **C5**.^[43,44a] Energies are given in $kcal\ mol^{-1}$.

tral (Figure 11), hydride and pyrrolide complexes **C5**·(**A**)² and **C3**·(**A**)² can readily interconvert, thus they are expected to participate in a mobile equilibrium.

Pathways commencing from the $\{N^{\wedge}N\}Ba$ silyl

We now consider the mechanistic branch that starts from $\{N^{\wedge}N\}Ba$ silyl compound **C6** (Scheme 6). The Ba–N amido σ -bond silanolysis of $\{N^{\wedge}N\}Ba$ pyrrolide **C3** has been studied as a plausible route that leads to the generation of **C6**. The process to start from the thermodynamically prevalent **C3**·(**A**)² sees the initial displacement of pyrrolidine by triphenylsilane, which leads to **C3**·**S**·**A** or, after the release of another adducted amine molecule, to **C3**·**S** encounter species and to proceed thereafter via a metathesis-type TS structure to furnish mono- or bis-amine adducts of **C6** (see Figure S3 in the Supporting Information). The exchange of the pyrrolide moiety for the silyl group at **C3**·(**S**)² requires a barrier of $21.3\ kcal\ mol^{-1}$ to overcome along the most accessible pathway (Figure 12), which in-

volves an additionally associated spectator amine molecule, but favours the $\{N^{\wedge}N\}Ba$ pyrrolide **C6**·(**A**)² ($\Delta G = 8.0\ kcal\ mol^{-1}$). It characterises the **C3**·(**A**)² + **S**(–**A**) \rightarrow **C6**·(**A**)² pathway to generate the $\{N^{\wedge}N\}Ba$ silyl complex as kinetically viable. Moreover, the **C6**·(**A**)² (and **C6**·**A**) precursors to silazane formation are somewhat more stable than the encounter species **C3**·**S**·**A** (and **C3**·**S**) that are involved in the alternative mechanistic branch for silazane formation, hence they can be expected to be populated in similar appreciable amounts.

The generation of silazane product **P** from the $\{N^{\wedge}N\}Ba$ silyl **C6**·(**A**)ⁿ preferably evolves through **TS**[**C6**·(**A**)²–**C5**·**P**·**A**], which describes concerted Ba–Si/N–H σ -bond-breaking metathesis in the presence of an adducted pyrrolidine spectator molecule (see Figure S4 in the Supporting Information). An additional pyrrolidine unit readily displaces the silazane **P** from **C5**·**P**·**A** to yield **C5**·(**A**)²,^[43] which renders the overall process virtually thermoneutral (relative to **C3**·(**A**)²). Despite its favourable thermodynamics, the prohibitively high barrier (in excess of $64\ kcal\ mol^{-1}$; Figure 13) makes the Si–N/Ba–H σ -bond-forming meta-

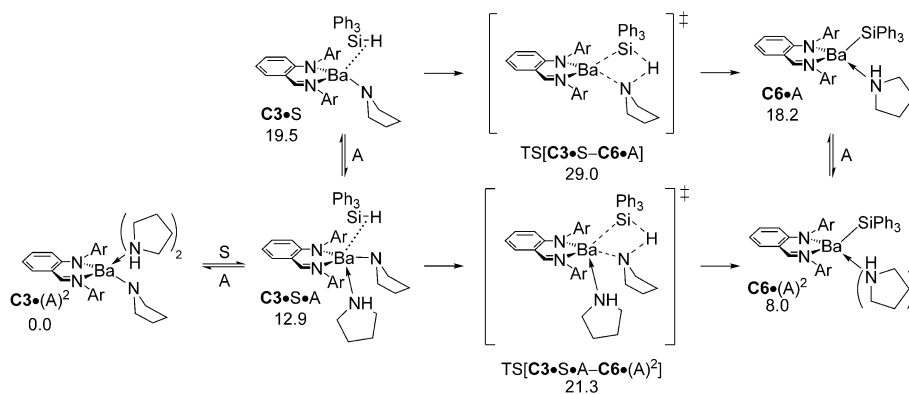


Figure 12. Ba–N pyrrolide α -bond protonolysis at **C3** by silane substrate **S**.^[43,44a] Energies are given in kcal mol⁻¹.

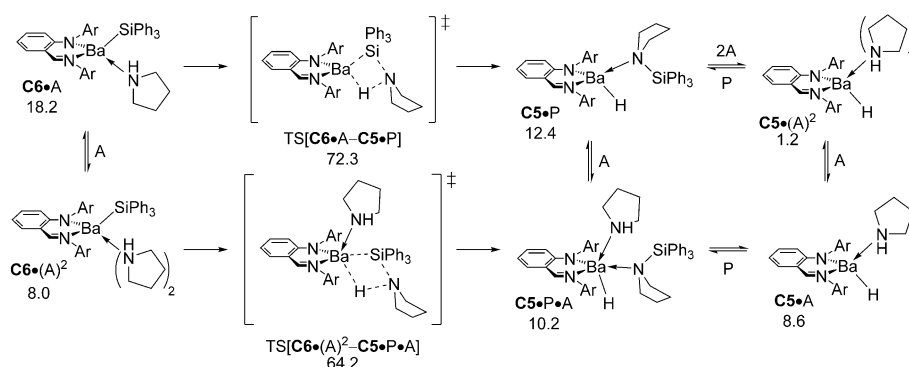


Figure 13. Ba–Si/N–H α -bond-breaking metathesis at $\{N^N\}Ba$ silyl compound **C6**.^[43,44a] Energies are given in kcal mol⁻¹.

thesis kinetically inaccessible. This result parallels the findings of a previous computational study on silane dehydrocoupling catalysed by some rare-earth compounds.^[45]

Moreover, the protonolysis of silane by the $\{N^N\}Ba$ hydride (see Figure S5 in the Supporting Information) that would follow thereafter, thereby regenerating the $\{N^N\}Ba$ silyl compound, is found to be more demanding energetically (Figure 14) when compared to the related protonolysis of pyrrolidine (Figure 11) via the alternative reaction branch. It is worth noting that the barrier associated with the prevalent $C5 \cdot S \cdot A \rightarrow C6 \cdot A + H_2(+A) \rightarrow C6 \cdot (A)_2$ pathway for silane protonolysis exceeds the overall barrier for silazane generation starting from the $\{N^N\}Ba$ pyrrolide complex **C3**.

Taking all these findings together, one can confidently dismiss the reaction branch that is initiated by the conversion of $\{N^N\}Ba$ pyrrolide **C3** (or $\{N^N\}Ba$ silylamide starting material **C2**·(T)²) into the $\{N^N\}Ba$ silyl **C6** and involves Ba–Si/N–H α -bond-breaking metathesis followed by silane protonolysis in the presence of an energetically prevalent pathway for stepwise silazane formation (Figures 10 and 11) with the $\{N^N\}Ba$ pyrrolide **C3** as the catalytically active compound. The turnover-limiting β -hydride elimination accounts for the rate acceleration observed for a silane with a *para* electron-withdrawing group, the negative charge build-up at silicon (given that a transient silicate intermediate featuring a hypervalent silicon centre is involved), which was indicated by a Hammett analysis

of substituted silanes, and also for the substantial primary KIE. Moreover, the Hammett analysis is inconsistent with those for other α -bond metathesis processes, which have not shown substantial charge accumulation in the TS,^[46] and provides further support for stepwise silazane formation. The DFT-assessed activation energy for turnover-limiting β -hydride elimination satisfactorily matches the empirically determined Eyring parameters.

These findings rationalise the distinct deviation in reactivity observed for Sr–pyrrolide **9-Sr** and bis-silanide **5-Sr** (see Table 1). On the one hand, **9-Sr** does not require further transformation prior to passing through the most accessible pathway, and thus is competent to catalyse the CDC. In contrast, an Ae silyl compound is seen to be incapable of effecting silazane formation and would thus make an initial conversion into an Ae amide indispensable for CDC catalysis to proceed. Complex **5-Sr** appears less effective in mediating such a transformation and/or subsequent nucleophilic attack and β -hydride elimination steps, hence rendering **5-Sr** catalytically inactive.

Although disilanes are not part of the observed product spectrum, we thought it would be informative to examine the rival homocoupling of Ph_3SiH (**S**) in the presence of $\{N^N\}Ba$ silyl **C6** (see Figure S6 in the Supporting Information). Both stepwise and concerted pathways are conceivable, but a stepwise pathway (dashed arrows in Scheme 6) that bears a formal similarity with the one shown in Figure 10 is energetically prev-

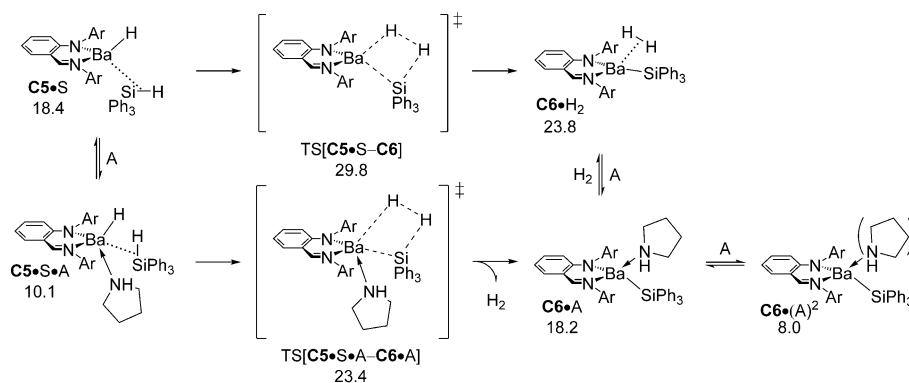


Figure 14. Protonolysis of the silane by the $\{N^{\wedge}N\}Ba$ hydride **C5**.^[43,44a] Energies are given in kcal mol^{-1} .

alent. As discovered for all the steps studied thus far, one associated amine spectator molecule **A** greatly facilitates silane homocoupling. In light of their formal analogy, it is tempting to compare the inherent propensity of the $\{NN\}Ba$ silyl **C6** and $\{NN\}Ba$ pyrrolide **C3** to nucleophilically attack triphenylsilane **S** and to effect β -H elimination from a five-coordinate silicon centre onto the alkaline earth. Considering the intrinsic barriers, Si–Si bond formation via $C6\cdot S \rightarrow C7\cdot A$ is more kinetically and thermodynamically demanding ($\Delta G_{\text{int}}^{\ddagger}/\Delta G_{\text{int}} = 13.8/9.9 \text{ kcal mol}^{-1}$ relative to $C6\cdot S\cdot A$; Figure 15) than $C3\cdot S\cdot A \rightarrow C4\cdot A$ N–Si bond formation ($\Delta G_{\text{int}}^{\ddagger}/\Delta G_{\text{int}} = 4.5/1.3 \text{ kcal mol}^{-1}$ relative to $C3\cdot S\cdot A$; Figure 10); this reflects the enhanced nucleophilicity of the pyrrolide N centre together with some steric constraints associated with silane homocoupling. By contrast, β -H elimination from the hypervalent silicon centre at transient silicate intermediates $C7\cdot A$ ($\Delta G_{\text{int}}^{\ddagger} = 5.4 \text{ kcal mol}^{-1}$ relative to $C7\cdot A$; Figure 15) and $C4\cdot A$ ($\Delta G_{\text{int}}^{\ddagger} = 4.8 \text{ kcal mol}^{-1}$ relative to $C4\cdot A$; Figure 10) is equally found highly facile. Despite its associated low intrinsic barrier, the fact that the nucleophilic attack of the $\{N^{\wedge}N\}Ba$ silyl is strongly uphill means that the second hydro-

gen transfer step determines the overall kinetics for the generation of Si_2Ph_6 and $\{N^{\wedge}N\}Ba$ hydride **C5**. Figure 15 reveals a prohibitively large overall barrier ($\Delta G^{\ddagger} = 36.2 \text{ kcal mol}^{-1}$ relative to $C3\cdot(A)^2$) for the rival silane homocoupling, which remains unachievable due to its non-competitive kinetic demands versus the most accessible stepwise pathway for silazane formation (Figures 10 and 11).

Comparison of $\{N^{\wedge}N\}Ae(NR_2)$ -mediated CDC reactions ($Ae = Ca, Sr, Ba$)

We start with the examination of the accessibility of the pathway for concerted silazane formation (shown in Scheme 5) for the Ca catalyst analogue. In contrast to the findings for barium, the TS structures for $Ae-N/Si-H$ σ -bond-breaking metathesis could be located for the more compact Ca centre; the key structural and energy features are summarised in Figures S7 and S8 (see the Supporting Information). Irrespective of whether a spectator pyrrolidine molecule participates in metathesis pathways, they are distinctly disfavoured kinetically

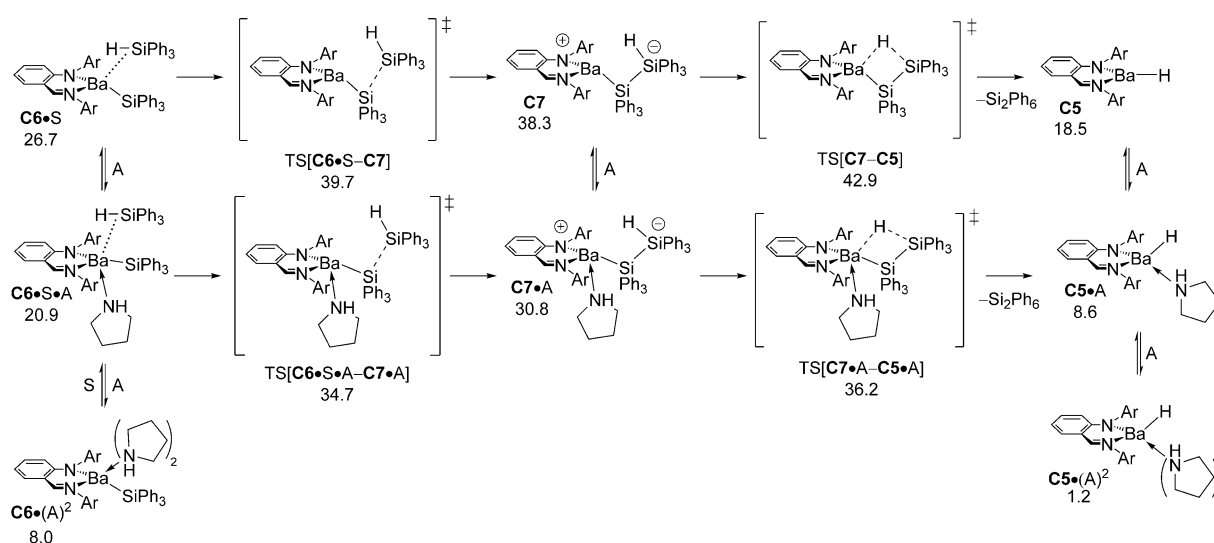


Figure 15. Nucleophilic attack of the $\{N^{\wedge}N\}Ba$ silyl **C6** at Ph_3SiH (**S**) together with subsequent hydrogen-atom transfer to barium at the transient intermediate **C7** to afford $\{N^{\wedge}N\}Ba$ hydride **C5** and the disilane product Si_2Ph_6 .^[43,44a] Energies are given in kcal mol^{-1} .

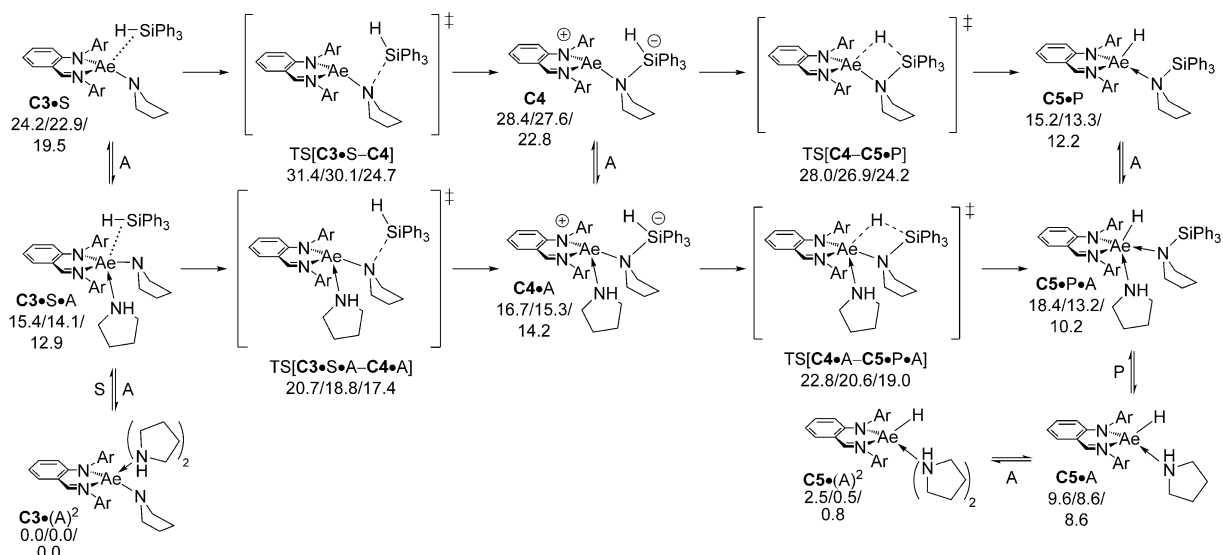


Figure 16. Nucleophilic attack of the $\{N^N\}Ae$ pyrrolide **C3** at the triphenylsilane **S** together with subsequent hydrogen transfer to the alkaline earth at the transient silicate intermediate **C4** to afford $\{N^N\}Ae$ hydride **C5** and the silazane (**P**) product ($Ae = Ca/Sr/Ba$).^[43,44] Energies are given in kcal mol⁻¹.

($\Delta\Delta G^\ddagger > 14$ kcal mol⁻¹; Figure S8 in the Supporting Information) relative to the corresponding pathway for stepwise silazane production (Figure 16). The pronounced energy gap between the stepwise and concerted pathways assessed for the Ca catalyst further corroborates our above conclusion that a σ -bond metathesis pathway remains inaccessible in the presence of an energetically prevalent stepwise pathway for all the alkaline earths studied.

Focusing exclusively on the prevalent silazane-generating pathways shown in Figures 10 and 11, we can analyse the extent to which the nature of the alkaline earth influences the relevant elementary steps. The generation of silazane **P** after consecutive nucleophilic attack and β -hydride elimination (Figure 16) and also subsequent conversion of the $\{N^N\}Ae$ hydride **C5** back into the catalytically competent $\{N^N\}Ae$ pyrrolide **C3** (Figure 17) benefit from involvement of an adducted pyrrolidine spectator molecule. In light of the increased accessibility of the alkaline earth upon going down the Group 2, the regular growth of the thermodynamic gap between the

C3•(A)² catalyst resting state and the **C3•S•A** precursor species for nucleophilic pyrrolide attack at **S** for ever more compact metal centres becomes understandable. The overall barrier associated with nucleophilic attack is likewise seen to increase regularly ($Ca > Sr > Ba$). Of particular note is the modest, but regular, decrease of the intrinsic activation energy for ever heavier alkaline earths ($\Delta G^\ddagger_{int} = 5.3, 4.7$ and 4.5 kcal mol⁻¹ for Ca, Sr and Ba, respectively, relative to **C3•S•A**) for the most accessible **C3•S•A** → **C4•A** pathway. Hence, limitations in the accessibility of the Ae centre together with variations in the Ae–N pyrrolide bond strength contribute towards the greater energy demands for lighter alkaline earths, with the former factor likely to be dominant. The subsequent β -hydride elimination appears to be turnover limiting for all the systems studied, and its total barrier follows a regular $Ca > Sr > Ba$ trend (Figure 16). It is perhaps instructive to look more closely at the intrinsic process energetics ($\Delta G^\ddagger_{int} = 7.4, 6.5$ and 6.1 kcal mol⁻¹ and $\Delta G_{int} = 3.0, -0.9$ and -2.7 kcal mol⁻¹ for Ca, Sr and Ba, respectively, relative to **C3•S•A**). Again a regular trend is displayed,

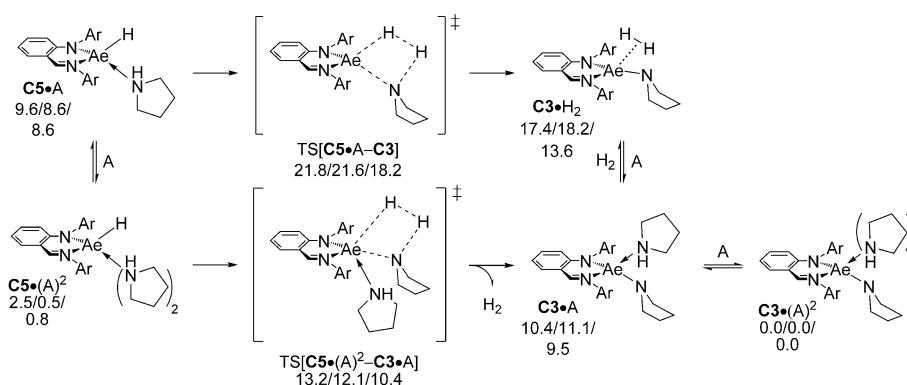


Figure 17. Protonolysis of pyrrolidine by the $\{N^N\}Ae$ hydride **C5** ($Ae = Ca/Sr/Ba$).^[43,44] Energies are given in kcal mol⁻¹.

which indicates that Ae–H bond formation is more kinetically and thermodynamically favourable upon going down Group 2. Hence, a sterically less restricted barium centre in combination with an increased aptitude for Ae–H bond formation give rise to the enhanced performance of the Ba catalyst relative to its lighter analogues.

The regeneration of the catalytically competent {N[^]N}Ae pyrrolide **C3** through protonolysis of pyrrolidine **A** by the {N[^]N}Ae hydride **C5** with concomitant release of H₂ (Figure 17) is significantly less kinetically demanding than stepwise silazane formation (Figure 16) for the studied family of iminoanilide alkaline-earth catalysts. Given that the thermodynamic force that drives this conversion is rather small, {N[^]N}Ae pyrrolide and {N[^]N}Ae hydride compounds can be expected to participate in a mobile equilibrium.

Conclusion

Alkaline-earth metal complexes constitute excellent chemoselective and versatile precatalysts for the production for a range of silazanes by CDC of amines and hydrosilanes. The scope of the reaction is large and includes diamines and di(hydrosilane)s. Characteristically, the catalytic activity increases substantially upon going down Group 2 according to (Mg ≪)Ca < Sr < Ba. This observation has been rationalised by DFT calculations, which show that greater accessibility of the metal centre and, to a lesser extent, decreasing Ae–N_{amide} bond strength down the Group 2 series, explain this trend. However, these conclusions solely apply to the CDC catalysis presented herein, and should not be extended to all Ae-mediated catalytic processes. The barium precatalysts Ba{CH(SiMe₃)₂}₂·(THF)₃ and Ba{N(SiMe₃)₂}₂·(THF)₂ display impressive performance, and because their synthesis is relatively facile they are recommended for the catalytic silazane formation.

The operative mechanism of the Ae-mediated CDC catalysis has been established with a high level of confidence following a kinetic analysis and DFT investigations of several rival pathways. In the presence of a catalytically competent iminoanilide Ba amide or Ba alkyl complex, pathways that involve a Ba silyl to mediate CDC catalysis or to furnish a disilane by-product are non-competitive. This is fully consistent with the experimental data: the formation of these species was not detected spectroscopically during the catalytic CDC reactions. Instead, complementary experimental and computational data provide conclusive evidence that CDC of amines and organosilanes follows a stepwise reaction path that consists of 1) N–Si bond-forming nucleophilic attack of the barium pyrrolide onto the silane, followed by 2) turnover-limiting hydrogen-atom transfer to the barium centre. A related mechanism was proposed for the CDC precatalyst {To^M}Mg{N(SiMe₃)₂}, for which nucleophilic attack was proposed to be rate-determining.^[20a]

The chemoselectivity and compatibility of these Ae precatalysts with monoamines, diamines, hydrosilanes and di(hydrosilane)s opens up a range of synthetic possibilities. The synthesis of original polycarbosilazanes by coupling of diamines and di(hydrosilane)s is an area where these Ae-mediated CDC processes can prove invaluable.^[32] Moreover, starting from an ini-

tial hydrosilane (e.g. Ph₃SiH, Et₃SiH), stoichiometric cascade couplings of diamines (H₂NCH₂–C₆H₄–CH₂NH₂, piperazine, etc.) or primary amines (e.g. BnNH₂) with hydrosilanes (e.g. Ph₂SiH₂) can yield unusual polysilazanes. Encoded and/or functionalised (macro)molecules can be prepared from judiciously selected bifunctional substrates, such as *p*-substituted arylsilanes. The Ae-promoted dehydrocoupling of amines with boranes and the coupling of silanes with phosphines are other natural extensions of this work. Our continued efforts will be detailed in forthcoming reports.

Experimental Section

General considerations

All manipulations were performed under an inert atmosphere by using standard Schlenk techniques or in a dry, solvent-free glovebox (Jacomex; O₂ < 1 ppm, H₂O < 5 ppm). AeI₂ beads (99.999%, Aldrich) was used as purchased. THF was distilled under argon from Na/benzophenone prior to use. Pentane, toluene, dichloromethane, and Et₂O were collected from MBraun SPS-800 purification alumina columns. Deuterated solvents (Eurisotop, Saclay, France) were stored in sealed ampoules over activated 3 Å molecular sieves and degassed by several freeze–thaw cycles. Ae{N(SiMe₃)₂}₂·(THF)₂,^[47] Ae{N(SiMe₃)₂}₂,^[47a] Ae{N(SiMe₂H)₂}₂,^[25,48] Ae{CH(SiMe₃)₂}₂·(THF)₃,^[49] {N[^]N}Ae{N(SiMe₃)₂}₂·(THF)_x,^[20c,25] and {N[^]N}Ae{CH(SiMe₃)₂}₂·(THF)_x,^[20c,25] (Ae = Ca, Sr or Ba) were prepared by following literature procedures.

NMR spectra were recorded with Bruker AM-400 or AM-500 spectrometers. All chemical shifts (δ) [ppm] were determined relative to the residual signal of the deuterated solvent and calibrated against SiMe₄. Assignment of the signals was assisted by 1D (¹H, ¹³C{¹H}) and 2D (COSY, HMBC, and HMQC) NMR experiments.

HRMS data were recorded with a Bruker MicrOTOF-Q II mass spectrometer equipped with an APCI (Atmospheric Pressure Chemical Ionisation) source in positive mode by direct introduction (ASAP—Atmospheric Solids Analysis Probe) at 370 °C.

Combustion analyses of **5-Sr** (C₄₈H₅₄O₃Si₂Sr, 822.75 g mol⁻¹), **5-Ba** (C₄₈H₅₄O₃Si₂Ba, 872.45 g mol⁻¹), **7-Ba** (C₄₃H₆₉N₃O₂Si₂Ba, 853.54 g mol⁻¹) and **9-Sr** (C₃₉H₅₆N₄Sr, 668.53 g mol⁻¹) were performed by with a Carlo–Erba analyzer. Despite repeated (>4) attempts on different batches of each of these compounds (including for crystals of **7-Ba**, which were also characterised by XRD), we were unable to obtain satisfactory and reproducible elemental analyses for these compounds. This can certainly be attributed to the extreme air- and moisture-sensitivity of the complexes, and also to the presence of substantial amounts of silicon in the samples leading to the formation of non-pyrolisable silicon carbides.

Complex 5-Sr

SrI₂ (300 mg, 0.8 mmol) was suspended in THF (10 mL) and stirred at 60 °C until dissolution was ensured (ca. 60 min). KSiPh₃ (500 mg, 1.6 mmol) was dissolved in THF (10 mL) and added dropwise via cannula to the SrI₂ solution at RT. The reaction mixture was stirred for 2.5 h and a white precipitate gradually appeared. The precipitate was removed by filtration and the solvent was removed under vacuum. Complex **5-Sr** was obtained as a yellow powder (230 mg, 32%) after washing with pentane (3 × 5 mL). ¹H NMR (C₆D₆, 500.1 MHz, 298 K): δ = 7.76 (m, 12H; *o*-C₆H₅), 7.47 (m, 12H; *m*-C₆H₅), 7.12 (m, 6H; *p*-C₆H₅), 3.24 (m, 12H; OCH₂CH₂), 1.24 ppm (m, 12H; OCH₂CH₂); ¹³C{¹H} NMR (C₆D₆, 125.8 MHz, 298 K): δ = 136.9 (*o*-C₆H₅),

136.4 (*m*-C₆H₅), 129.9 (*p*-C₆H₅), 68.4 (OCH₂CH₂), 25.6 ppm (OCH₂CH₂).
²⁹Si{¹H} NMR (C₆D₆, 79.5 MHz, 298 K): δ = -12.14 ppm.

Complex 5-Ba

Ba₂ (328 mg, 0.8 mmol) was suspended in THF (10 mL) and stirred at 60 °C until dissolution was ensured (ca. 60 min). KSiPh₃ (500 mg, 1.6 mmol) was dissolved in THF (10 mL) and added dropwise via cannula to the Ba₂ solution at RT. The reaction mixture was stirred for 2.5 h and a white precipitate gradually appeared. The precipitate was removed by filtration and the solvent was removed under vacuum. Complex **5-Ba** was obtained as an orange powder (600 mg, 86%) after washing with pentane (3 × 5 mL). ¹H NMR (C₆D₆, 500.1 MHz, 298 K): δ = 7.68 (m, 12H; *o*-C₆H₅), 7.46 (m, 12H; *m*-C₆H₅), 6.96 (m, 6H; *p*-C₆H₅), 3.54 (m, 12H; OCH₂CH₂), 1.40 ppm (m, 12H; OCH₂CH₂); ¹³C{¹H} NMR (C₆D₆, 125.8 MHz, 298 K): δ = 136.63 (*o*-C₆H₅), 130.4 (*m*-C₆H₅), 125.9 (*p*-C₆H₅), 68.3 (OCH₂CH₂), 25.7 ppm (OCH₂CH₂); ²⁹Si{¹H} NMR (C₆D₆, 79.5 MHz, 298 K): δ = -12.11 ppm.

Complex 7-Ba

Anhydrous Ba₂ beads (446 mg, 1.14 mmol) were suspended in THF (10 mL) and activated at 60 °C for 60 min. KN(SiMe₂H)₂ (373 mg, 2.18 mmol) and {N[^]N}H (480 mg, 1.09 mmol) were dissolved in THF (10 mL) and the solution was added dropwise via cannula to the Ba₂ solution at RT. The reaction mixture was stirred for 2.5 h and a white precipitate gradually appeared. The precipitate was removed by filtration and the solvent was pumped off under vacuum. Complex **7-Ba** was extracted with pentane (3 × 5 mL) and isolated as orange crystals (521 mg, 56%) by crystallisation at -27 °C. Crystals suitable for X-ray diffraction studies were selected from this batch. ¹H NMR (C₆D₆, 500.1 MHz, 298 K): δ = 8.04 (s, 1H; CH=N), 7.28 (d, ³J(H,H) = 7.6 Hz, 2H; arom-*H*), 7.19 (m, 1H; arom-*H*), 7.12 (m, 3H; arom-*H*), 7.00 (m, 1H; arom-*H*), 6.92 (td, ³J(H,H) = 8.6 Hz, ⁴J(H,H) = 1.8 Hz, 1H; arom-*H*), 6.28 (t, ³J(H,H) = 8.2 Hz, 1H; arom-*H*), 6.22 (d, ³J(H,H) = 8.7 Hz, 1H; arom-*H*), 4.71 (br, ¹J(H,Si) = 160 Hz, 2H; Si(CH₃)₂H), 3.36 (m, 10H; OCH₂CH₂ (8H) and CH(CH₃)₂ (2H)), 3.18 (q, ³J(H,H) = 6.8 Hz, 2H; CH(CH₃)₂), 1.31 (m, 20H; OCH₂CH₂ (8H) and CH(CH₃)₂ (12H)), 1.23 (d, ³J(H,H) = 6.7 Hz, 6H; CH(CH₃)₂), 1.17 (d, ³J(H,H) = 6.7 Hz, 6H; CH(CH₃)₂), 0.24 ppm (br, 12H; Si(CH₃)₂H). ¹³C{¹H} NMR (C₆D₆, 125.8 MHz, 298 K): δ = 169.2 (CH=N), 158.0 (N=CH-*i*-C₆H₄), 149.5 (ArN-*i*-C₆H₃), 146.6 (CH=N-*i*-C₆H₃), 144.6 (N-*i*-C₆H₄), 140.8 (ArN-*o*-C₆H₃), 139.6 (N=CH-*o*-C₆H₄), 133.7 (N-*o*-C₆H₄), 125.7 (CH=N-*o*-C₆H₃), 125.3 (ArN-*m*-C₆H₃), 124.8 (CH=N-*m*-C₆H₃), 124.7 (N=CH-*m*-C₆H₄), 118.6 (CH=N-*i*-C₆H₃), 118.4 (ArN-*p*-C₆H₃), 110.5 (N=CH-*p*-C₆H₄), 68.9 (OCH₂CH₂), 29.2 (CH(CH₃)₂), 28.5 (CH(CH₃)₂), 26.4 (CH(CH₃)₂), 26.2 (CH(CH₃)₂), 25.7 (OCH₂CH₂), 25.4 (CH(CH₃)₂), 23.8 (CH(CH₃)₂), 5.1 ppm (Si(CH₃)₂H); FTIR (Nujol in KBr plates): $\tilde{\nu}$ = 2964 (s), 2887 (s), 2004 (s), 1984 (sh), 1601 (sh), 1579 (m), 1380 (s), 1377 (s), 1359 (w), 1338 (s), 1234 (s), 1151 (s), 1097 (s), 1037 (w), 1004 (m), 947 (s), 916 (s), 887 (w), 827 cm⁻¹ (m).

Complex 9-Sr

{N[^]N}Sr{CH(SiMe₃)₂}(THF)₂ (250 mg, 0.29 mmol) was dissolved in pentane (10 mL). Pyrrolidine (69 μL, 0.86 mmol) was diluted in pentane (5 mL) and the solution was added dropwise via cannula to the precatalyst solution. The reaction mixture was stirred for 2.5 h at RT. At the end of the reaction the solution was stored at -27 °C and **9-Sr** was isolated as an orange solid after precipitation from solution (102 mg, 51%). ¹H NMR (C₆D₆, 500.1 MHz, 298 K): δ = 8.07 (s, 1H; CH=N), 7.25 (m, 3H; arom-*H*), 7.08 (m, 3H; arom-*H*), 7.01 (m, 1H; arom-*H*), 6.79 (td, ³J(H,H) = 6.8 Hz, ⁴J(H,H) = 3.4 Hz, 1H; arom-

H), 6.21 (m, 2H; arom-*H*), 3.23 (br, 2H; CH(CH₃)₂), 3.05 (br, 2H; CH(CH₃)₂), 2.49 (br, 8H; HNCH₂CH₂ (4H) and SrNCH₂CH₂ (4H)), 1.27 (br, 8H; HNCH₂CH₂ (4H) and SrNCH₂CH₂ (4H)), 1.23 (d, ³J(H,H) = 6.9 Hz, 6H; CH(CH₃)₂), 1.11 (m, 12H; CH(CH₃)₂), 1.06 (d, ³J(H,H) = 6.7 Hz, 6H; CH(CH₃)₂), 0.94 ppm (brs, 1H; HN(CH₂)₄); ¹³C{¹H} NMR (C₆D₆, 125.8 MHz, 298 K): δ = 172.58 (CH=N), 160.0 (N=CH-*i*-C₆H₄), 149.7 (ArN-*i*-C₆H₃), 143.8 (CH=N-*i*-C₆H₃), 140.7 (ArN-*o*-C₆H₃), 139.5 (CH=N-*o*-C₆H₃), 133.5 (N-*i*-C₆H₄), 126.4 (CH=N-*o*-C₆H₃), 124.7 (N=CH-*m*-C₆H₄), 124.4 (N=CH-*p*-C₆H₄), 119.6 (ArN-*p*-C₆H₃), 116.4 (N-*o*-C₆H₄), 111.7 (CH=N-*p*-C₆H₃), 49.2 (BaNCH₂CH₂), 34.5 (HNCH₂CH₂), 29.3 (BaNCH₂CH₂), 28.7 (CH(CH₃)₂), 26.5 (CH(CH₃)₂), 25.7 (HNCH₂CH₂), 24.6 (CH(CH₃)₂), 23.8 (CH(CH₃)₂), 22.0 (CH(CH₃)₂), 22.7 ppm (CH(CH₃)₂).

NMR-scale generation of complex 10-Ba

In a glovebox, {N[^]N}Ba{N(SiMe₃)₂}(THF)₂ (10 mg, 0.011 mmol) was added to an NMR tube. The NMR tube was stored in a Schlenk tube, which was removed from the glovebox and connected to a Schlenk manifold. Standard Schlenk techniques were used for subsequent manipulations. C₆D₆ (0.5 mL) and pyrrolidine (≈ 2.0 μL, 0.022 mmol) were added to the NMR tube. The NMR tube was sealed and shaken vigorously, and then put into an oil bath at 25 °C for 2 h. The reaction mixture was directly analysed by ¹H NMR spectroscopy. ¹H NMR (C₆D₆, 500.1 MHz, 298 K): δ = 8.05 (s, 1H; CH=N), 7.19 (d, ³J(H,H) = 7.6 Hz, 2H; arom-*H*), 7.16 (m, 1H; arom-*H*), 7.11 (m, 4H; arom-*H*), 6.91 (td, ³J(H,H) = 8.6 Hz, ⁴J(H,H) = 1.8 Hz, 1H; arom-*H*), 6.29 (t, ³J(H,H) = 8.0 Hz, 1H; arom-*H*), 6.22 (d, ³J(H,H) = 8.8 Hz, 1H; arom-*H*), 3.50 (br, 2H; CH(CH₃)₂), 3.27 (hept, ³J(H,H) = 6.8 Hz, 2H; CH(CH₃)₂), 2.41 (br, 8H; HN(CH₂)₄), 1.33 (d, ³J(H,H) = 7.0 Hz, 6H; CH(CH₃)₂), 1.27 (br, 20H; HNCH₂CH₂ (8H) and CH(CH₃)₂ (12H)), 1.23 (d, ³J(H,H) = 6.7 Hz, 6H; CH(CH₃)₂), 0.60 (br, 2H; HN(CH₂)₄), 0.21 ppm (s, 18H; Si(CH₃)₃); ¹³C{¹H} NMR (C₆D₆, 125.8 MHz, 298 K): δ = 169.3 (CH=N), 158.0 (N=CH-*i*-C₆H₄), 149.8 (ArN-*i*-C₆H₃), 146.6 (CH=N-*i*-C₆H₃), 141.0 (ArN-*o*-C₆H₃), 139.6 (CH=N-*o*-C₆H₃), 133.9 (N-*i*-C₆H₄), 126.0 (CH=N-*o*-C₆H₃), 124.9 (N=CH-*m*-C₆H₄), 124.9 (N=CH-*p*-C₆H₄), 124.7 (ArN-*p*-C₆H₃), 118.6 (N-*o*-C₆H₄), 111.1 (CH=N-*p*-C₆H₃), 50.3 (HNCH₂CH₂), 30.5 (CH(CH₃)₂), 29.4 (CH(CH₃)₂), 28.8 (HNCH₂CH₂), 26.4 (CH(CH₃)₂), 26.2 (CH(CH₃)₂), 25.7 (CH(CH₃)₂), 24.0 (CH(CH₃)₂), 5.8 ppm (Si(CH₃)₃).

Typical procedure for catalytic CDC reactions

The following standard protocol was used for the catalytic CDC reactions. In a glovebox, precatalyst **1-9** (0.005 mmol, 1 equiv) was loaded into an NMR tube. The NMR tube was stored in a Schlenk tube, which was then removed from the glovebox and connected to a double-manifold Schlenk line. Standard Schlenk techniques were used for subsequent manipulations. The amine (*n* × 0.005 mmol, *n* equiv) and silane (*n* × 0.005 mmol, *n* equiv) were added to the NMR tube via syringe. The NMR tube was sealed, removed from the Schlenk tube, shaken vigorously, then placed in an oil bath at 298 or 333 K. After the required time period, the reaction was quenched by addition of "wet" C₆D₆ at RT. Substrate conversion was determined from the ¹H NMR spectrum of the reaction mixture, by comparing the relative intensities of characteristic resonances of the substrates and products. All silazanes were isolated as solids after quenching the reaction mixture, evaporating the volatile compounds, washing the residue with pentane and drying it to constant weight.

Procedure for kinetic measurements

The following protocol was used for catalytic CDC reactions monitored by ^1H NMR spectroscopy. In a glovebox, precatalyst **6-Ba** and Ph_3SiH were loaded into an NMR tube. The NMR tube was stored in a Schlenk tube, which was then removed from the glovebox and connected to a double-manifold Schlenk line. Pyrrolidine and C_6D_6 (0.5 mL) were added to the NMR tube via syringe. The NMR tube was sealed, removed from the Schlenk tube, vigorously shaken, and inserted into the probe of a Bruker AM 500 NMR spectrometer preheated to the required temperature. The reaction kinetics were monitored starting from this point using the *multi zgvd* command of the TopSpin package ($\text{D1}=0.2\text{ s}$; $\text{DS}=0$; $\text{NS}\geq 8$). The conversion was determined on the basis of amine consumption over the course of three or more half-lives, by comparing the relative intensities of characteristic resonances of the substrates and products.

X-ray diffraction crystallography

Crystals of **7-Ba** suitable for X-ray diffraction analysis were obtained by recrystallisation from pentane at -27°C . Diffraction data were collected at 150(2) K by using a Bruker APEX CCD diffractometer with graphite-monochromated $\text{Mo}_{\text{K}\alpha}$ radiation ($\lambda=0.71073\text{ \AA}$). A combination of ω and Φ scans was carried out to obtain a unique data set. The crystal structures were solved by direct methods, the remaining atoms were located from difference Fourier synthesis followed by full-matrix least-squares refinement based on F2 (programmes SIR97 and SHELXL-97).^[50] Carbon- and oxygen-bound hydrogen atoms were placed at calculated positions and forced to ride on the attached atom. All non-hydrogen atoms were refined with anisotropic displacement parameters. The locations of the largest peaks in the final difference Fourier map calculation, as well as the magnitude of the residual electron densities, were of no chemical significance. Relevant collection and refinement data are given in the Supporting information. CCDC 1426816 (**7-Ba**) contains the supplementary crystallographic data for this paper. These data are provided free of charge by The Cambridge Crystallographic Data Centre.

Computational methodology

All calculations based on Kohn–Sham DFT^[51] were performed by using the program package TURBOMOLE^[52] with flexible triple- ζ basis sets. The Becke–Perdew (BP86)^[53] generalised gradient approximation (GGA) functional within the RI- J integral approximation^[54] in conjunction with appropriate auxiliary basis sets was used for structure optimisation. Empirical dispersion corrections by Grimme (D3 with Becke–Johnson damping)^[55] were used to account for non-covalent interactions. For Ba and Sr, we used the Stuttgart–Dresden scalar-relativistic effective core potential (SDD, 46 and 28 core electrons for Ba and Sr, respectively)^[56] in combination with the (7s7p5d1f)/[6s4p3d1f] (def2-TZVPP) valence basis set;^[57] Ca was treated by the (17s12p4d)/[6s5p3d] (def2-TZVPP) all-electron basis set.^[57] All remaining elements were represented by Ahlrich’s valence triple- ζ TZVP basis set^[58a–b] with polarisation functions on all atoms. Final potential energies were obtained by single-point calculations on BP86-D3 optimised structures with the B97-D^[59] GGA functional (together with D3(BJ) empirical dispersion correction)^[55] in conjunction with the aforementioned ECP/basis set for the Ae atoms and a def2-TZVP^[54] basis set for all remaining elements (B97-D3/(SDD + def2-TZVP)//BP86-D3/(SDD + TZVP)). A large integration grid (m4 in TURBOMOLE notation) and tight SCF convergence criteria have been used. The validity of the computa-

tional protocol employed for reliably mapping the energy landscape of Ae-mediated hydroamination has been substituted before,^[39,41g] and this allowed mechanistic conclusions with substantial predictive value to be drawn.

The reaction pathways were explored by a chain-of-states method^[60] as implemented in the module *woelfling* in the TURBOMOLE suite of programmes, which makes use of reasonably chosen reactant and product structures to approximate the minimum-energy path (MEP). The reactant and product states to be linked to the associated transition state were identified. The approximate saddle points connected with the MEP were subjected to an exact localisation of the TS structures. No structural simplification of any of the key species involved was imposed, nor have symmetry constraints have been imposed in any case. The DFT calculations simulated the authentic reaction conditions by treating the bulk effects of the benzene solvent by a consistent continuum model in the form of the conductor-like screening model for realistic solvents (COSMO-RS)^[61] as implemented in COSMOtherm.^[62] This solvation model includes continuum electrostatic and also solvent-cavitation and solute-solvent dispersion effects through surface-proportional terms, and it also refers properly to a 1 M standard state. The free solvation enthalpy was assessed with the aid of COSMO-RS at the BP86/(SDD + def2-TZVP)//BP86-D3/(SDD + TZVP) level of approximation. Geometry optimisation and frequency calculations were also performed at the BP86-D3/(SDD + SV(P))^[58c] level to confirm the nature of all optimised key structures and to determine the thermodynamic parameters (298 K, 1 atm) under the conventional ideal-gas, rigid-rotor and quantum-mechanical harmonic-oscillator approximations. This level of basis-set quality is known to be reliable for the assessment of structural parameters and vibrational frequencies,^[63] thus it allows an affordable and accurate determination of thermodynamic state functions. As far as the vibrational partition function is concerned, all frequencies below 60 cm^{-1} were replaced by a value of 60 cm^{-1} to correct for the quantum-mechanical harmonic-oscillator approximation for such normal modes (the quasi-harmonic approximation),^[64] and thermochemical contributions to enthalpy and entropy were computed from the resulting partition function. The entropy contributions for condensed-phase conditions were estimated based on computed gas-phase entropies (without any scaling applied) by employing Okuno’s procedure.^[65] The mechanistic conclusions drawn in this study were based on the Gibbs free-energy profile of the catalytic cycle assessed at the B97-D3(COSMO-RS)/(SDD + def2-TZVP) level of approximation for experimental condensed-phase conditions. The calculated structures were visualised by employing the StruEd program,^[66] which was also used for the preparation of 3D molecular drawings.

Acknowledgements

This work was sponsored by the French Ministry for Higher Education and Research (Ph.D. grant to C.B.). The authors thank Stephen Boyer (London Metropolitan University) for performing the elemental analyses.

Keywords: alkaline-earth metals · barium · density functional calculations · cross-dehydrocoupling · reaction mechanisms

[1] a) J. F. Harrod, *Coord. Chem. Rev.* **2000**, *206–207*, 493; b) R. Waterman, *Chem. Soc. Rev.* **2013**, *42*, 5629; c) E. M. Leitao, T. Jurca, I. Manners, *Nat. Chem.* **2013**, *5*, 817; d) R. L. Melen, *Chem. Soc. Rev.* DOI: 10.1039/c5cs00521c.

- [2] a) T. Wideman, L. G. Sneddon, *Chem. Mater.* **1996**, *8*, 3; b) J. E. Mark, H. R. Allcock, R. West, *Inorganic Polymers*, 2nd ed., Oxford University Press, **2005**; c) T. Baumgartner, R. Réau, *Chem. Rev.* **2006**, *106*, 4681; d) A. Nunns, J. Gwyther, I. Manners, *Polymer* **2013**, *54*, 1269; e) A. K. Franz, S. O. Wilson, *J. Med. Chem.* **2013**, *56*, 388.
- [3] M. Lappert, P. P. Power, A. Protchenko, A. Seeber, *Metal Amide Chemistry*, Wiley, Chichester, **2009**.
- [4] L. F. Fieser, M. Fieser, *Reagents in Organic Chemistry*, Wiley, New York, **1967**.
- [5] a) Y. Tanabe, M. Murakami, K. Kitaichi, Y. Yoshida, *Tetrahedron Lett.* **1994**, *35*, 8409; b) Y. Tanabe, T. Misaki, M. Kurihara, A. Iida, Y. Nishii, *Chem. Commun.* **2002**, 1628.
- [6] a) P. J. Kociński, *Protecting Groups*, 3rd ed., Thieme, Stuttgart, **2005**, pp. 595–599; b) D. W. Robbins, T. A. Boebel, J. F. Hartwig, *J. Am. Chem. Soc.* **2010**, *132*, 4068; c) S. Itagaki, K. Kamata, K. Yamaguchi, N. Mizuno, *Chem. Commun.* **2012**, *48*, 9269; d) C. D. F. Königs, M. F. Müller, N. Aiguabella, H. F. T. Klare, M. Oestreich, *Chem. Commun.* **2013**, *49*, 1506; e) L. Greb, S. Tamke, J. Paradies, *Chem. Commun.* **2014**, *50*, 2318.
- [7] a) D. Seyferth, G. H. Wiseman, C. Prud'homme, *J. Am. Ceram. Soc.* **1983**, *66*, C-13; b) D. Seyferth, G. H. Wiseman, *J. Am. Ceram. Soc.* **1984**, *67*, C-132; c) Y. D. Blum, K. B. Schwartz, R. M. Laine, *J. Mater. Sci.* **1989**, *24*, 1707; d) D. Seyferth, J. M. Schwark, R. M. Stewart, *Organometallics* **1989**, *8*, 1980; e) E. Duguet, M. Schappacher, A. Soum, *Macromolecules* **1992**, *25*, 4835; f) N. R. Dando, A. J. Perrotta, C. Strohmman, R. M. Stewart, D. Seyferth, *Chem. Mater.* **1993**, *5*, 1624; g) M. Birot, J.-P. Pilot, J. Dunoguès, *Chem. Rev.* **1995**, *95*, 1443; h) D. Su, Y. Li, F. Hou, X. Yan, *J. Am. Ceram. Soc.* **2014**, *97*, 1311.
- [8] R. Fessenden, J. S. Fessenden, *Chem. Rev.* **1961**, *61*, 361.
- [9] a) L. H. Sommer, J. D. Citron, *J. Org. Chem.* **1967**, *32*, 2470; b) J. F. Blandez, I. Esteve-Adell, M. Alvaro, H. García, *Catal. Sci. Technol.* **2015**, *5*, 2167.
- [10] a) Y. Blum, R. M. Laine, *Organometallics* **1986**, *5*, 2081; b) C. Biran, Y. D. Blum, R. Glaser, D. S. Tse, K. A. Youngdahl, R. M. Laine, *J. Mol. Catal.* **1988**, *48*, 183; c) C. K. Toh, H. T. Poh, C. S. Lim, W. Y. Fan, *J. Organomet. Chem.* **2012**, *717*, 9.
- [11] W. D. Wang, R. Eisenberg, *Organometallics* **1991**, *10*, 2222.
- [12] E. J. Matarasso-Tchiroukhine, *Chem. Soc. Chem. Commun.* **1990**, 681.
- [13] H. Q. Liu, J. F. Harrod, *Can. J. Chem.* **1992**, *70*, 107.
- [14] a) H. Q. Liu, J. F. Harrod, *Organometallics* **1992**, *11*, 822; b) for the related coupling of hydrosilanes and hydrazines, see: J. He, H. Q. Liu, J. F. Harrod, R. Hynes, *Organometallics* **1994**, *13*, 336.
- [15] L. K. Allen, R. García-Rodríguez, D. S. Wright, *Dalton Trans.* **2015**, *44*, 12112.
- [16] A. E. Nako, W. Chen, A. J. P. White, M. R. Crimmin, *Organometallics* **2015**, *34*, 4369.
- [17] a) K. Takaki, T. Kamata, Y. Miura, T. Shishido, K. Takehira, *J. Org. Chem.* **1999**, *64*, 3891; b) K. Takaki, K. Komeyama, K. Takehira, *Tetrahedron* **2003**, *59*, 10381; c) F. Buch, S. Harder, *Organometallics* **2007**, *26*, 5132; d) W. Xie, H. Hu, C. Cui, *Angew. Chem. Int. Ed.* **2012**, *51*, 11141; *Angew. Chem.* **2012**, *124*, 11303.
- [18] J. X. Wang, A. K. Dash, J. C. Berthet, M. Ephritikhine, M. S. Eisen, *J. Organomet. Chem.* **2000**, *610*, 49.
- [19] T. Tsuchimoto, Y. Iketani, M. Sekine, *Chem. Eur. J.* **2012**, *18*, 9500.
- [20] a) J. F. Dunne, S. R. Neal, J. Engelkemier, A. Ellern, A. D. Sadow, *J. Am. Chem. Soc.* **2011**, *133*, 16782; b) M. S. Hill, D. J. Liptrot, D. J. MacDougall, M. F. Mahon, T. P. Robinson, *Chem. Sci.* **2013**, *4*, 4212; c) C. Bellini, J.-F. Carpentier, S. Tobisch, Y. Sarazin, *Angew. Chem. Int. Ed.* **2015**, *54*, 7679; *Angew. Chem.* **2015**, *127*, 7789.
- [21] The NMR spectroscopic data were unambiguous regarding the formulation and structure of **9-Sr**, which clearly contained one coordinated pyrrolidine molecule. On the other hand, we could not clearly assess the exact formulation of its Ba congener **9-Ba**: the ¹H NMR spectrum of the complex obtained suggested the presence of one to two pyrrolidine molecules, and we were not able to remove the doubt as to its actual composition. Elemental analysis was not informative, and we failed in our attempts to obtain X-ray quality crystals (see Figure S8 in the Supporting Information for details).
- [22] R. J. P. Corriu, C. Guérin, *J. Chem. Soc. Chem. Commun.* **1980**, 168.
- [23] The pale-yellow Ca derivative Ca(SiPh₃)₂(THF)₄ ($\delta_{295\text{Si}} = -13.99$ ppm), in which the metal is stabilised by four THF molecules instead of three as in **5-Sr** and **5-Ba**, was recently reported: a) V. Leich, T. P. Spaniol, L. Maron, J. Okuda, *Chem. Commun.* **2014**, *50*, 2311; b) V. Leich, T. P. Spaniol, J. Okuda, *Inorg. Chem.* **2015**, *54*, 4927. The difference in the ²⁹Si NMR chemical shifts between Ca(SiPh₃)₂(THF)₄ and **5-Sr/5-Ba** ($\delta_{295\text{Si}} = -12.14$ and -12.11 ppm) reflects the presence of one extra THF molecule in the Ca complex, and these values altogether hint at highly ionic Ae...Si bonding. For other examples of Ae silanides, see: c) W. Teng, U. Englich, K. Ruhlandt-Senge, *Angew. Chem. Int. Ed.* **2003**, *42*, 3661; *Angew. Chem.* **2003**, *115*, 3789; d) D. J. Liptrot, M. Arrowsmith, A. L. Colebatch, T. J. Hadlington, M. S. Hill, G. Kociok-Köhn, M. F. Mahon, *Angew. Chem. Int. Ed.* **2015**, *54*, 15280; *Angew. Chem.* **2015**, *127*, 15495.
- [24] Y. Sarazin, D. Roşca, V. Poirier, T. Roisnel, A. Silvestru, L. Maron, J.-F. Carpentier, *Organometallics* **2010**, *29*, 6569.
- [25] B. Liu, T. Roisnel, J.-F. Carpentier, Y. Sarazin, *Chem. Eur. J.* **2013**, *19*, 13445.
- [26] In a similar fashion, we checked that the NMR-scale reaction (C₆D₆, 298 K) of pyrrolidine (2 equiv) with bis-alkyl complex **4-Ba** releases CH₂(SiMe₃)₂ quantitatively, whereas the evolution of free HN(SiMe₃)₂ during the reaction with bis-amide **1-Ba** cannot be detected spectroscopically. See the Supporting Information (Figure S9–S11) for details.
- [27] B. Liu, T. Roisnel, J.-F. Carpentier, Y. Sarazin, *Chem. Eur. J.* **2013**, *19*, 2784.
- [28] a) O. Michel, K. W. Törnroos, C. Maichle-Mössmer, R. Anwander, *Chem. Eur. J.* **2011**, *17*, 4964; b) O. Michel, K. W. Törnroos, C. Maichle-Mössmer, R. Anwander, *Eur. J. Inorg. Chem.* **2012**, 44.
- [29] B. Liu, T. Roisnel, J.-F. Carpentier, Y. Sarazin, *Angew. Chem. Int. Ed.* **2012**, *51*, 4943; *Angew. Chem.* **2012**, *124*, 5027.
- [30] Under identical conditions, the magnesium complexes did not afford significant catalytic activity. For instance, [Mg(N(SiMe₃)₂)₂]₂ only afforded 2% conversion of the substrates after 15 h reaction at 298 K with [pyrrolidine]₀ = 4.0 m and [pyrrolidine]₀/[Ph₃SiH]₀/[Mg]₀ = 400:400:1.
- [31] Under identical conditions to those given in Table 1, entry 6, the bis-silazido Ba complex **5-Ba** also proved totally inactive. On the other hand, the Ba analogue of the pyrrolido complex **9-Sr** fully converted the substrates under the same conditions (i.e. those corresponding to Table 1, entry 8). However, due to the uncertainty as to the identity of this Ba species (see ref. [21]), we have considered these results in the simplest qualitative manner.
- [32] Dehydropolymerisation reactions involving the catalytic coupling of (d)amines and di(hydrosilane)s are specific applications and will be reported elsewhere: C. Bellini, C. Orione, J.-F. Carpentier, Y. Sarazin, *Angew. Chem. Int. Ed.* **2016**, 10.1002/anie.201511342 in press.
- [33] For instance, under discriminating conditions ([diamine]₀/[silane]₀/[**1-Ba**]₀ = 20:40:1, [diamine]₀ = 0.2 m, 298 K, 2.5 h), substrate conversion in the coupling of *N,N'*-dimethylethylenediamine with Ph₃SiH catalysed by **1-Ba** reached 43, 45 and 40% in C₆D₆, C₆D₅Cl and C₆D₆/1,2-C₆H₄F₂, respectively.
- [34] This disappointing result subsequently led us to assess the feasibility of the dehydrocoupling between Bn₂NH and Ph₃SiH. Very low conversions to Bn₂N–SiPh₃ were recorded with **1-Ba** (3%) and **4-Ba** (7%) after 12 h at 333 K, with [Bn₂NH]₀/[Ph₃SiH]₀/[Ba]₀ = 20:20:1 and [Bn₂NH]₀ = 0.1 m in C₆D₆. We are unable to explain the very poor reactivity of these dibenzyl-substituted amines in CDC reactions other than by arguing that steric factors may be unfavourable: the formation of the Ba–NBn₂ species required for catalytic turnover (see computational investigations) may be sterically prohibited for these congested amines.
- [35] The maximal kinetic isotope effect was calculated according to Equations (3) and (4):
- $$k_{\text{Si-D}}/k_{\text{Si-H}} = e^{-\lambda} \quad (3)$$
- $$\lambda = (h c v_{\text{Si-H}})/(2 k_{\text{B}} T) \times \{1 - (\mu_{\text{SiH}}/\mu_{\text{SiD}})^{1/2}\} \quad (4)$$
- in which *h* is the Planck constant, *c* is the speed of light, *k_B* is the Boltzmann constant, μ_{SiH} and μ_{SiD} are the relevant effective masses, and *v_{Si-H}* is the wavenumber for the stretching vibration of the N–H bond in the FTIR spectrum of the amine recorded at the temperature *T*. See: P. Atkins, J. de Paula, *Physical Chemistry*, 7th ed., Oxford University Press, Chichester **2002**, pp. 888–889. We measured $\nu_{\text{Si-H}} = 2117$ cm⁻¹ at *T* = 290.5 K, giving $k_{\text{Si-H}}/k_{\text{Si-D}} = 4.35$.
- [36] Arrhenius analysis for the same data set gave *E_a* = 16.2(23) kcal mol⁻¹.
- [37] For the values of sigma, see: C. G. Swain, E. C. Lupton, *J. Am. Chem. Soc.* **1968**, *90*, 4328.
- [38] B. Liu, T. Roisnel, J.-P. Guégan, J.-F. Carpentier, Y. Sarazin, *Chem. Eur. J.* **2012**, *18*, 6289.
- [39] S. Tobisch, *Chem. Eur. J.* **2014**, *20*, 8988.

- [40] B. Liu, J.-F. Carpentier, Y. Sarazin, *Chem. Eur. J.* **2012**, *18*, 13259.
- [41] a) S. Datta, M. T. Gamer, P. W. Roesky, *Organometallics* **2008**, *27*, 1207; b) M. Arrowsmith, M. S. Hill, G. Kociok-Köhn, *Organometallics* **2009**, *28*, 1730; c) M. Arrowsmith, M. S. Hill, G. Kociok-Köhn, *Organometallics* **2011**, *30*, 1291; d) J. Jenter, R. Köppe, P. W. Roesky, *Organometallics* **2011**, *30*, 1404; e) M. Arrowsmith, M. R. Crimmin, A. G. M. Barrett, M. S. Hill, G. Kociok-Köhn, P. A. Procopiu, *Organometallics* **2011**, *30*, 1493; f) M. Arrowsmith, M. S. Hill, G. Kociok-Köhn, *Organometallics* **2014**, *33*, 206; g) S. Tobisch, *Chem. Eur. J.* **2015**, *21*, 6765.
- [42] C. Brinkmann, A. G. M. Barrett, M. S. Hill, P. A. Procopiu, S. Reid, *Organometallics* **2012**, *31*, 7287.
- [43] a) Substrate association and dissociation at the various intermediates is presumably facile and rapid equilibria are expected. b) Examination by a linear-transit approach gave no indication that such processes are associated with a significant enthalpy barrier.
- [44] a) The prevalent pyrrolidine bis-amine adduct $C3(A)^2$ of the catalytically competent $[N^{\wedge}N]Ba\{N(CH_2)_4\}$ pyrrolide complex (with the appropriate number of substrate, silazane product or THF molecules) was chosen as the reference for the relative free energies [$kcal\ mol^{-1}$]. b) Free energies are given for Ca, Sr and Ba analogues of the relevant key species.
- [45] a) L. Perrin, O. Eisenstein, L. Maron, *New J. Chem.* **2007**, *31*, 549; b) L. Perrin, L. Maron, O. Eisenstein, T. D. Tilley, *Organometallics* **2009**, *28*, 3767.
- [46] M. E. Thompson, S. M. Baxter, A. R. Bulls, B. J. Burger, M. C. Nolan, B. D. Santarsiero, W. E. Schaefer, J. E. Bercaw, *J. Am. Chem. Soc.* **1987**, *109*, 203.
- [47] a) M. Westerhausen, *Inorg. Chem.* **1991**, *30*, 96; b) J. M. Boncella, C. J. Coston, J. K. Cammack, *Polyhedron* **1991**, *10*, 769; c) Y. Sarazin, R. H. Howard, D. L. Hughes, S. M. Humphrey, M. Bochmann, *Dalton Trans.* **2006**, 340.
- [48] N. Romero, S.-C. Roşca, Y. Sarazin, J.-F. Carpentier, L. Vendier, S. Mallet-Ladeira, C. Dinoi, M. Etienne, *Chem. Eur. J.* **2015**, *21*, 4115.
- [49] M. R. Crimmin, A. G. M. Barrett, M. S. Hill, D. J. MacDougall, M. F. Mahon, P. A. Procopiu, *Chem. Eur. J.* **2008**, *14*, 11292.
- [50] a) G. M. Sheldrick, SHELXS-97, Program for the Determination of Crystal Structures, University of Göttingen, Germany, **1997**; b) G. M. Sheldrick, SHELXL-97, Program for the Refinement of Crystal Structures, University of Göttingen, Germany, **1997**.
- [51] R. G. Parr, W. Yang, *Density-Functional Theory of Atoms and Molecules*, Oxford University Press, Oxford, **1989**.
- [52] a) R. Ahlrichs, M. Bär, M. Häser, H. Horn, C. Kölmel, *Chem. Phys. Lett.* **1989**, *162*, 165; b) O. Treutler, R. Ahlrichs, *J. Chem. Phys.* **1995**, *102*, 346; c) R. Ahlrichs, F. Furche, C. Hättig, W. Klopper, M. Sierka, F. Weigend, TURBOMOLE, version 6.6, University of Karlsruhe, Karlsruhe, Germany, **2014**, <http://www.turbomole.com>.
- [53] a) P. A. M. Dirac, *Proc. R. Soc. London Ser. A* **1929**, *123*, 714; b) J. C. Slater, *Phys. Rev.* **1951**, *81*, 385; c) S. Vosko, L. Wilk, M. Nusiar, *Can. J. Phys.* **1980**, *58*, 1200; d) A. D. Becke, *Phys. Rev. A* **1988**, *38*, 3098; e) J. P. Perdew, *Phys. Rev. B* **1986**, *33*, 8822.
- [54] a) O. Vahtras, J. Almlöf, M. W. Feyereisen, *Chem. Phys. Lett.* **1993**, *213*, 514; b) K. Eichkorn, O. Treutler, H. Öhm, M. Häser, R. Ahlrichs, *Chem. Phys. Lett.* **1995**, *242*, 652.
- [55] a) S. Grimme, J. Anthony, S. Ehrlich, H. Krieg, *J. Chem. Phys.* **2010**, *132*, 154104; b) S. Grimme, S. Ehrlich, L. Goerigk, *J. Comput. Chem.* **2011**, *32*, 1456; c) <http://toc.uni-muenster.de/DFTD3/getd3.html>.
- [56] D. Andrae, U. Häußermann, M. Dolg, H. Stoll, H. Preuß, *Theor. Chim. Acta* **1990**, *77*, 123.
- [57] a) F. Weigend, R. Ahlrichs, *Phys. Chem. Chem. Phys.* **2005**, *7*, 3297; b) F. Weigend, *Phys. Chem. Chem. Phys.* **2006**, *8*, 1057.
- [58] a) A. Schäfer, C. Huber, R. Ahlrichs, *J. Chem. Phys.* **1994**, *100*, 5829; b) K. Eichkorn, F. Weigend, O. Treutler, R. Ahlrichs, *Theor. Chem. Acc.* **1997**, *97*, 119; c) A. Schäfer, C. Huber, R. Ahlrichs, *J. Chem. Phys.* **1992**, *97*, 2571.
- [59] a) S. Grimme, *J. Comput. Chem.* **2006**, *27*, 1787; b) A. D. Becke, *J. Chem. Phys.* **1997**, *107*, 8554.
- [60] P. Plessow, *J. Chem. Theory Comput.* **2013**, *9*, 1305.
- [61] a) A. Klamt, G. Schüürmann, *J. Chem. Soc. Perkin Trans. 2* **1993**, 799; b) A. Klamt, *J. Phys. Chem.* **1995**, *99*, 2224; c) F. Eckert, A. Klamt, *AIChE J.* **2002**, *48*, 369; d) A. Klamt, F. Eckert, W. Arlt, *Annu. Rev. Chem. Biomol. Eng.* **2010**, *1*, 101; e) A. Klamt, *WIREs Comput. Mol. Sci.* **2011**, *1*, 699.
- [62] F. Eckert, A. Klamt, COSMOtherm, Version C3.0, Release 13.01, COSMOlogic GmbH & Co. KG, Leverkusen, Germany, **2012**.
- [63] W. Koch, M. C. Holthausen, *A Chemist's Guide to Density Functional Theory*, 2nd ed., Wiley-VCH, Weinheim, **2001**.
- [64] a) J. A. Keith, R. J. Nielsen, J. Oxgaard, W. A. Goddard, *J. Am. Chem. Soc.* **2007**, *129*, 12342; b) R. F. Ribeiro, A. V. Marenich, C. J. Cramer, D. G. Truhlar, *J. Phys. Chem. B* **2011**, *115*, 14556.
- [65] Y. Okuno, *Chem. Eur. J.* **1997**, *3*, 212.
- [66] For further details, see <http://www.struked.de>.

Received: October 27, 2015

Published online on February 11, 2016